International Scientific-Technical and Production Journal

The Paton WELDING JOURNAL

May 2004 # 5

English translation of the monthly «Avtomaticheskaya Svarka» (Automatic Welding) journal published in Russian since 1948

Founders: *E.O. Paton Electric Welding Institute of the NAS of Ukraine*
International Association «Welding»

Publisher: *International Association «Welding»*

Address:
E.O. Paton Electric Welding Institute,
International Association «Welding»,
11, Bozhenko str., 03680, Kyiv, Ukraine
Tel.: (38044) 227 67 57
Fax: (38044) 268 04 86
E-mail: journal@paton.kiev.ua
http://www.nas.gov.ua/pwj

State Registration Certificate
KV 4790 of 09.01.2001

Subscriptions:
$460, 12 issues per year,
postage and packaging included.
Back issues available.

CONTENTS

COMPUTER CONTROL OF ELECTRON BEAM WELDING WITH MULTI-COORDINATE DISPLACEMENTS OF THE GUN AND WORKPIECE

B.E. PATON[1], O.K. NAZARENKO[1], V.M. NESTERENKOV[1], A.A. MOROZOV[2], V.V. LITVINOV[2] and V.V. KAZIMIR[2]
[1]E.O. Paton Electric Welding Institute, NASU, Kiev, Ukraine
[2]Institute of Problems of Mathematical Machines and Systems, NASU, Kiev, Ukraine

A new approach is considered to construction of control systems of EBW machines with a multi-coordinate displacement system. Its main feature is implementation of a visual method of development of welding programs for complex three-dimensional structures.

Keywords: *electron beam welding, computer control, welding displacements, virtual representation, visual design, automatic training, butt following*

Aerospace industry, nuclear and power engineering, electronics and precision electromechanics are the best developed fields of EBW application in production [1]. This is exactly the welding process which the designers have in mind when designing complex-shaped workpieces. Over the last years the need for a simultaneous multi-coordinate displacement of the electron gun and workpiece being welded has become obvious, which cannot be implemented without computer control.

Modern EBW machines have distributed computer systems, which incorporate interconnected by interface buses, but separately functioning devices of CNC type, which is the modern analog of numerical program control, and programmable logic controller (PLC) type. Welding programs proper are executed by CNC processor, and programs of control of the support equipment — by PLC processor.

It is known [2] that CNC programs are written in G-codes (Figure 1), and are a sequence of blocks (code lines), in which the coordinates of the point, to which it is necessary to move, as well as the method and parameters of interpolation during this displacement, are assigned for each section of the trajectory.

In EBW programs the following is assigned in the block: values of welding current CW, focusing current CF, process scan and deflection set when the final point of the programmed section of the trajectory has been reached, and displacement speed in this section. Additional tasks, related to axes synchronizing, maintaining a stable speed, etc., are assigned by special commands, which are also stored as separate code blocks. With simultaneous use of several coordinates, when the final trajectory is a complex spatial curve, the traditional procedure envisages development of a displacement program, using the drawing of the workpiece to be welded, and CAD/CAM system with a special postprocessor, capable of converting the trajectory designed in the CAD/CAM system into its machine representation in the form of G-codes for a specific CNC. Depending on the complexity of the trajectory, duration of preparation of such a program can be from several hours up to several days or weeks.

It should be further taken into account that the operator will also spend some time directly at the machine, in order to adapt the earlier designed program to the actual workpiece, allowing for inaccuracies of its fabrication and placing into the welding position. And while such a correction is simple enough, when using just linear coordinates (X, Y,

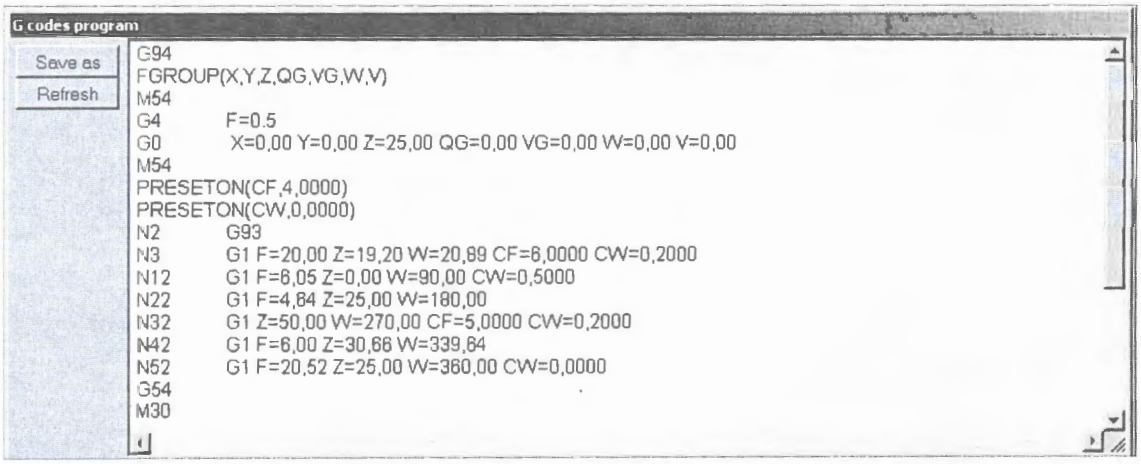

Figure 1. Fragment of EBW program written in G-codes

Z), adaptation becomes extremely complicated at formation of the trajectory by simultaneous linear and angular displacements. Therefore, with preservation of the tendency for use of highly accurate CNC systems, the goal was to create the development software built into these systems, which would allow the operator himself to develop programs of welding complex structures in a short time and without involving any additional resources. This problem required a new approach to construction of the system of EBW process control. The main feature of this approach is application of a high-level operator interface with advanced development software, providing a visual method of EBW program design.

The paper gives the main results of application of such an approach.

Architecture of the computer control system. Let us consider some complex-shaped 3D structures and programmed displacement of the gun and workpiece, required for their welding. The Table (see inset between pp. 2 and 3) gives illustrations of complex-shaped structures, where welding requires having at least four simultaneously controlled axes, taking into account the need to ensure beam perpendicularity to workpiece surface. Figure 2 gives designations of coordinate axes and welding displacements, the set of which allows such workpieces to be welded. Hardware architecture of the computer control system, which allows implementation of these welding displacements, is shown in Figure 3. As is seen from the Figure, in addition to the traditional [3] computing system, combining CNC and PLC, we also use:

• higher level of human machine interface (HMI), which is operator interface for visual design of working programs and welding process monitoring;

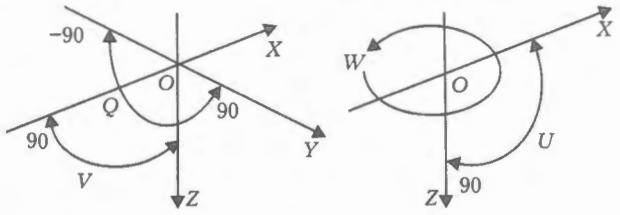

Figure 2. System of coordinate axes and welding displacements: X, Y, Z — linear axes of gun displacement; Q — angle of gun displacement; V — angle of inclination; W — angle of displacement of the table faceplate; U — angle of table inclination

• additional computer, which independently of other microprocessor units, performs butt recognition by workpiece surface image, received from RASTR following system, and together with HMI computer supports the functions of automatic teaching, correction and following of the butt.

Principle of operation of RASTR following system [4] is based on measurement of current of secondary emission electrons, formed at cyclic (with 300 ms period) scanning of the working zone of the workpiece by a sharply-focused low power beam during short moments (up to 5 ms) of welding process interruption. Image of workpiece surface is formed by signals from the sensor of secondary emission electrons, mounted on the electron gun in the direct vicinity of the welding site. Brightness levels of the scanned surface sections, measured and digitized by the following system, are stored in the computer as an image frame (matrix), and after a special program processing are reproduced in a separate window of RASTR monitor. Today the following system allows only flat images to be produced. Interface modules (IM) provide exchange of control signals with the machine equipment. In particular, current control and synchronizing of interac-

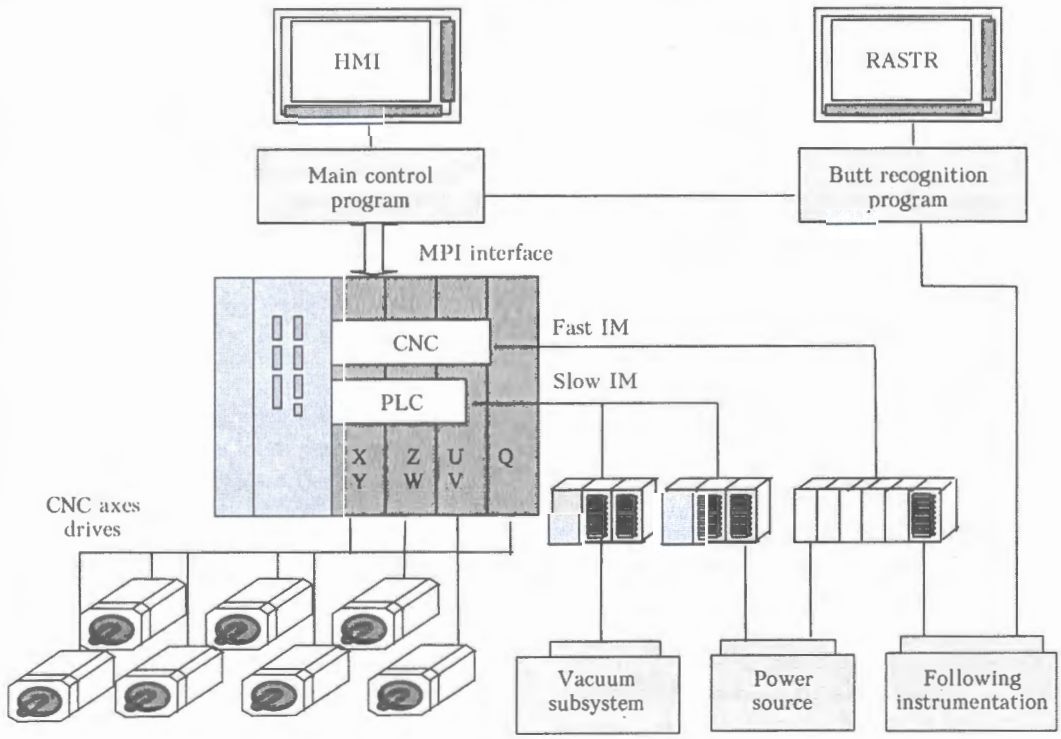

Figure 3. Hardware architecture of the computer control system

tion with RASTR following system are performed through fast HM with CNC operation rate, with up to 75 μs delay.

Proposed architecture allows eliminating the traditional programming of welding in G-codes and implementing EBW program control by a sequential performance of the following processes: construction of a 3D virtual representation of the situation inside the vacuum chamber; selection of the initial point of butt trajectory using the developed virtual representation; teaching the displacement system to follow the butt trajectory; automatic following of the butt during performance of welding to compensate the arising welding deformations.

Virtual representation of the item and welding trajectory. The operator needs the virtual 3D representation of the workpiece inside the vacuum chamber to select the characteristic points and assign the correct angular orientation of the gun during visual design of the trajectory.

Developed software for virtual representation allows, in particular:

- developing 3D images of workpieces (see the Table in the inset);
- represent the actual arrangement of the workpiece and gun inside the vacuum chamber;
- change the scale and angle of observation of the formed image for its more convenient and complete presentation;
- represent the location of the programmed welding trajectory on the workpiece surface;
- assign admissible areas of gun displacement and perform automatic monitoring of its displacements to avoid damaging the workpiece or in-chamber equipment;
- follow on the workpiece surface the position of the electron beam relative to the assigned trajectory during performance of welding.

Workpiece images are formed by the machine operator himself from a basic set of autofigures and are represented in HMI monitor in a 3D space (x, y, z). However, representation of beam trajectory on workpiece surface in this space in the reality produced as a result of welding displacement in a multi-dimensional space (X, Y, Z, V, Q, W, U) requires transforming seven-coordinate vectors describing the trajectory points, into 3D vectors.

With this purpose, in order to allow for the angles of rotation and inclination of the gun, let us find additional vector $\mathbf{A} = (-rX, 0, rZ + D)$, where rX is the distance along coordinate X from beam axis to axis of gun inclination; rZ is the distance from the axis of gun rotation to its edge; D is the distance from gun edge to the workpiece surface. Further on for each point we will rotate vector **A** around the axis of gun rotation in plane YZ through angle Q, and then around the axis of gun inclination in plane XZ through angle V. As a result, we obtain coordinates of a point relative to the center of rotation and inclination of the gun (x_1, y_1, z_1).

In order to allow for angles of rotation and inclination of the table, let us find additional vector $\mathbf{B} = (X_{rot}, Y_{rot}, Z_{rot} + dZ_{rot})$, where X_{rot}, Y_{rot}, Z_{rot} are the coordinates of the table center in the basic system of coordinates; dZ_{rot} is the distance from the axis of table inclination to its surface. Further on by moving the coordinate center to the end of vector **B** and rotating the vector (X, Y, Z) of each point around the axis of table rotation in plane XY through angle W, we obtain point (x_2, y_2, z_2), and then by rotation around the axis of the table inclination in plane XZ through angle U, we obtain point (x_3, y_3, z_3).

As a result, the basic coordinates of points, according to which the points will be represented inside the vacuum chamber, are recalculated by the following expression:

$$(x, y, z) = (X + X_{rot} + x_1 + x_2 + x_3, Y + Y_{rot} + y_1 + y_2 + y_3, Z + Z_{rot} + z_1 + z_2 + z_3). \quad (1)$$

Visual design of the welding program. At design of simple, for instance, one-dimensional welds, the operator may assign the coordinates of welding displacement points in the form of a table. Automatic teaching procedure is envisaged to write the program of making a weld of a complex 3D shape. This procedure uses the image of the butt of edges to be welded (Figure 4, *a*, see inset between pp. 2 and 3). The butt in this image is shown as a dark line against a lighter surface of the workpiece. The cross shows the point of location of the electron beam center. By manually moving the gun, the operator combines the electron beam with the initial point of the butt of edges to be welded, and issues a command for automatic teaching, which is implemented as a result of joint operation of RASTR and HMI computers. During motion in the direction initially specified by the operator, the recognition program finds the butt (blue line) in each new frame, and determines the vector of displacement (yellow line, coming out of the cross) to a new point of the trajectory located in the middle of the butt.

Algorithm of recognition implements the segmentation method with incremental marking of butt points [5]. To increase the efficiency of the method, it was modified by considering not the individual pixels, but whole groups of them. After continuity testing, the first pixel, belonging to a direction with average brightness level closest to that of the butt, is recorded in the butt area. The entire set of image frame points belonging to the butt, is found in such a way. The linear displacement vector is calculated, proceeding from the condition of provision of the required accuracy of the beam hitting the butt middle of not less that 0.1 mm. CNC executes displacement to a new point with linear interpolation, and issues a signal for determination of the coordinates of the next point to the RASTR computer. As a result, the cross is again located on the butt line. Automatic teaching will be completed, if the next found point coincides with the previous point (butt end has been reached) or initial point (for a closed trajectory).

Виды изделий и требуемые перемещения
Kinds of products and required displacements

Вид изделия Kinds of products	Описание стыка Description of the butt	Требуемые перемещения Required welding displacements
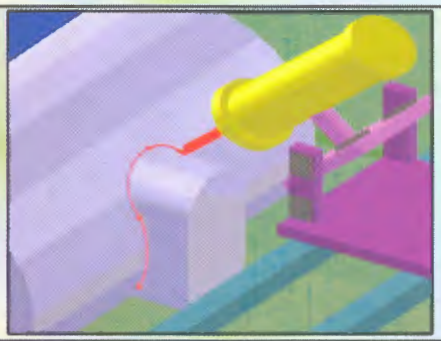	Патрубок овальной формы вваривается в протяженный толстостенный цилиндр Oval-shaped branchpipe is welded into an extended thick-walled cylinder	Поворот изделия, перемещение пушки по двум линейным осям и ее наклон Rotation of the products, gun displacement along two linear axes and its inclination
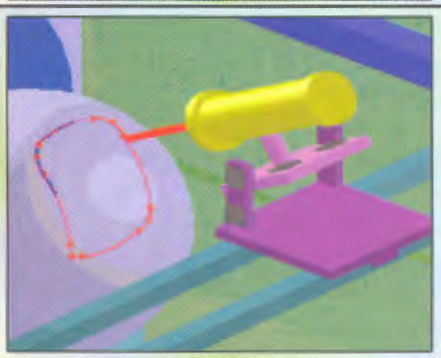	Вваривание прямоугольного сегмента с закругленными углами в поверхность шара Welding-in of a rectangular segment with rounded-off corners into a spherical surface	Наклон или поворот пушки, перемещение пушки по трем линейным осям Gun tilting or rotation, gun displacement along three linear axes
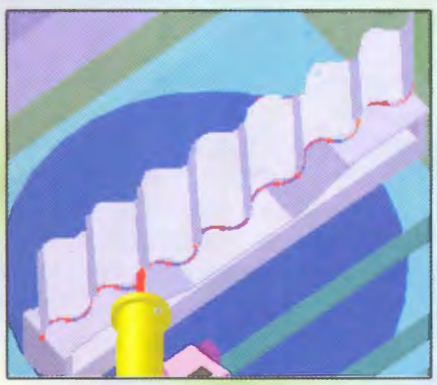	Приваривание гофрированного листа к трапецеидальному основанию Welding a corrugated sheet to a trapezoidal base	Поворот и перемещение пушки по трем линейным осям Gun rotation and displacement along three linear axes

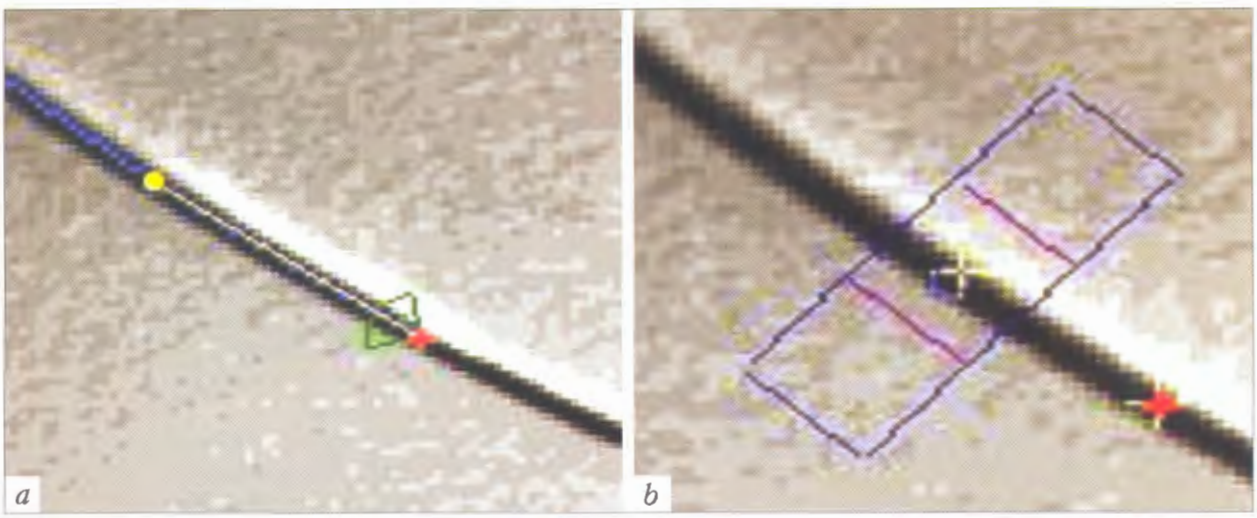

Рис. 4. Вид окна с изображением поверхности изделия на мониторе РАСТР при автоматическом обучении (*a*) и при слежении за стыком (*b*)

Fig. 4. View of a window with the image of product surface in RASTR monitor at automatic training (*a*) and at butt following (*b*)

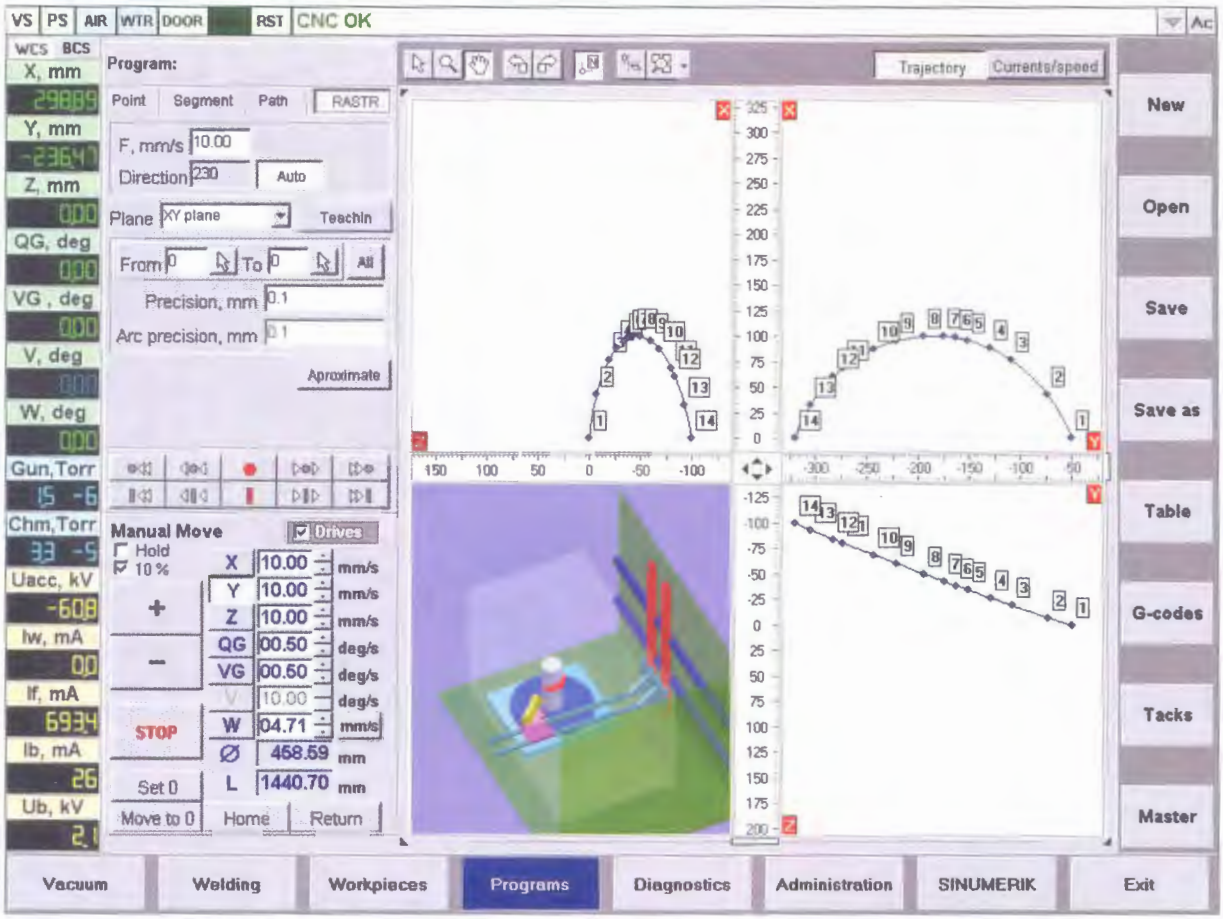

Рис. 5. Вид экрана монитора HMI в режиме визуального проектирования программы ЭЛС

Fig. 5. View of HMI monitor screen in the mode of visual design of the EBW program

Рис. 6. Установка КЛ-115 для ЭЛС с реализованной семикоординатной системой перемещения

Fig. 6. KL-115 machine for EBW with implemented 7 axes displacement system

The trajectory which is formed during automatic teaching, is represented in the basis coordinate planes (Figure 5, see inset between pp. 2 and 3) for the case of performance of an inclined semi-circumferential weld on a cylindrical body by four-coordinate displacement of the gun, namely rotation and displacement by three linear axes. As new points of the trajectory are found, they are connected with the previous section of straight lines. The thus produced piecewise-linear model of the actual butt does not take into account its geometrical features and contains an excess amount of points (the greater the butt curvature, the more points are required for its piecewise-linear approximation), which may be reduced by conducting additional approximation by the operator's command.

A feature of the implemented algorithm of additional approximation is the fact that the equations of the line or circular arc, produced by the least squares method, are corrected so that the coordinates of the initial and final points remained unchanged. When checking the possibility of linear approximation of a selected section of the trajectory, consisting of n points, coefficients of a section of the straight line are given by the following formula:

$$a = \frac{s_{xy} - s_x s_y}{s_{x^2} - s_x s_x}, \quad b = \frac{s_{x^2} s_y - s_x s_{xy}}{s_{x^2} - s_x s_x}, \qquad (2)$$

where

$$s_x = \sum_{i=0}^{n-1} x_i; \quad s_{x^2} = \sum_{i=0}^{n-1} x_i^2; \quad s_y = \sum_{i=0}^{n-1} y_i; \quad s_{xy} = \sum_{i=0}^{n-1} x_i y_i.$$

If the plotted regression line does not provide the required accuracy, an attempt is made to select an arc of a circle, approximating the selected section of the trajectory. Unknown coefficients a, b and c, which are used for calculation of the radius of circumference $R = \sqrt{c + a^2 + b^2}$, are given by the following system of equations:

$$\begin{cases} s_{y^2} b + s_{xy} a + s_y c = s_{y^3} + s_{x^2 y}, \\ s_{xy} b + s_{x^2} a + s_x c = s_{xy^2} + s_{x^3}, \\ s_y b + s_x a + nc = s_{y^2} + s_{x^2}, \end{cases} \qquad (3)$$

where

$$s_x = \sum_{i=0}^{n-1} x_i; \quad s_{x^2} = \sum_{i=0}^{n-1} x_i^2; \quad s_{x^3} = \sum_{i=0}^{n-1} x_i^3; \quad s_y = \sum_{i=0}^{n-1} y_i;$$

$$s_{xy} = \sum_{i=0}^{n-1} x_i y_i; \quad s_{x^2 y} = \sum_{i=0}^{n-1} x_i^2 y_i;$$

$$s_{xy^2} = \sum_{i=0}^{n-1} x_i y_i^2; \quad s_{y^3} = \sum_{i=0}^{n-1} y_i^3; \quad s_{y^2} = \sum_{i=0}^{n-1} y_i^2.$$

Considering that the initial and final points of the interpolation section are taken to be fixed, coordinates of the circumference center are additionally corrected. If the calculated circular approximation does not meet the required accuracy, either, it is automatically rejected, and the length of the analyzed section of the trajectory is reduced by one point. Furtheron the approximation process is repeated.

In addition to performance of the above additional approximation, the operator can correct the obtained trajectory manually by varying the point coordinates, methods of interpolation (linear or circular) in the selected sections of the trajectory, adding new points to the already existing trajectory or eliminating some points in the already obtained trajectory. The operator also assigns and corrects all the process parameters of welding as point parameters, including the beam and focusing currents, speed of welding displacement from point to points, etc.

The visually designed welding program, when it is started in the automatic mode, without operator participation, is converted into a sequence of G-codes executed by CNC. This program can be viewed in a separate window of HMI monitor (see Figure 1).

A mode of automatic following of the butt directly during the process of welding by the composed program, is envisaged, in view of the possible welding distortions of the workpiece. The frame of the image of the butt formed during butt following (Figure 4, *b*, see inset between pp. 2 and 3) shows the zone of butt detection, as well as the actual and calculated point of location of the center of the electron beam. The zone of butt detection is moved forward relative to the current welding area, where the weld pool forms. The found deviations of the trajectory from the butt are compensated by beam deflections, which are stored by the program and may be memorized at repeated (for instance, cosmetic) passes.

The above architecture of construction of the control system and method of visual design of programs of control of multi-coordinate displacements have already been implemented in production machines (Figure 6, see inset between pp. 2 and 3).

In conclusion it should be noted that in the considered paper the approach to construction of EBW machines of a new generation, based on application of distributed computer architecture with a developed human-machine interface allowed solving the entire range of problems of control of multi-coordinate displacements. Developed methods and algorithms have ensured automatic teaching of complex trajectories and butt following during welding, have greatly expanded the capabilities of visual design of welding programs, and thus have improved the quality and effectiveness of EBW application in fabrication of complex 3D structures.

1. Nazarenko, O.K., Kajdalov, A.A., Kovbasenko, S.N. et al. (1987) *Electron beam welding*. Ed. by B.E. Paton. Kiev: Naukova Dumka.
2. Sosonkin, V.L. (1991) *Program control of process equipment*. Leningrad: Mashinostroenie.
3. Schiller, S., Heisig, U., Panzer, S. (1988) *Electron beam technology*. New York: Wiley&Sons.
4. Nazarenko, O.K., Shapoval, V.I., Loskutov, G.A. et al. (1993) Observation of the electron beam welding process and automatic seam tracking. *Avtomatich. Svarka*, **5**, 35–38.
5. Buzovsky, O.V., Boldak, A.O., Mohamed Rumi, M.Kh. (2001) *Computerized processing of images*. Kiev: Kornijchuk.

CALCULATION-EXPERIMENTAL METHOD FOR EVALUATION OF RESIDUAL LIFE OF WELDED JOINTS IN STEAM PIPELINES

F.A. KHROMCHENKO and **R.N. KALUGIN**
OJSC «VTI», Moscow, Russian Federation

Calculation-experimental methodological approach to evaluation of residual life of steam pipelines on the basis of long-time strength and structural state (microdamage) of metal of welded joints under creep conditions is considered.

Keywords: *power plants, welded steam pipelines, long-time strength, creep, residual life, safety factor for strength*

The methodology developed and applied by the Open Joint Stock Company «VTI» to address problems associated with residual life of welded joints in steam pipelines [1–4] is based on a combination of calculation-experimental methods employed to estimate residual life on the basis of long-time strength of metal and structural state (microdamage) of welded joints under creep conditions (Figures 1 and 2).

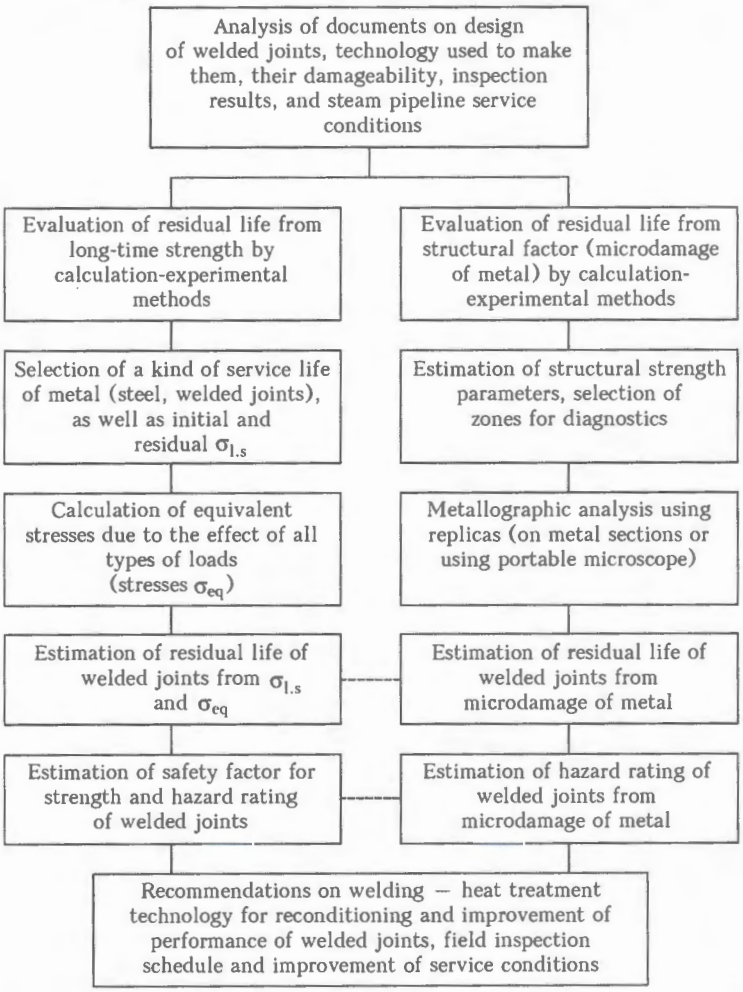

Figure 1. General algorithm for evaluation of residual life of welded joints in steam pipelines by calculation-experimental methods

Calculation-experimental method based on long-time strength. The method has a number of versions, which are chosen depending upon the availability of information on heat resistance of metal: standardised (according to [5]) rated values of long-time strength of the base metal, i.e. steel, $[\sigma_{l.s}^{b.m}] = 1.5[\sigma]$, where $[\sigma]$ are the permissible stresses for steel (deviation is ± 20 % of the rated values); reference long-time strength of welded joints $\sigma_{l.s}^{w.j}$ (deviation is ± 10 %), established from the data of long-term research conducted by «VTI» [4]; and actual residual life of welded joints $\sigma_{l.s(a.r.l)}^{w.j}$, found from the results of long-time strength tests of specimens of welded joints cut from an active steam pipeline. Permissible stresses $[\sigma]$ are stresses assigned for a given steel grade to be operated at a given temperature during a design lifetime of the steam pipeline. The $[\sigma]$ values are specified by strength design standards [5].

Calculated equivalent stresses σ_{eq} are determined as total stresses caused by all types of loads (internal pressure, weight loads, self-compensation due to thermal expansion) using a simplified [1–4] and/or refined approach [5], but necessarily with allowance for design of welded joints and technology used to make them. The design and technology peculiarities include decrease in wall thickness due to boring of the internal surface of pipe elements to place a jar washer, probable extra weakening of the weld metal in creep $\sigma_{\omega}^{w.m} = 0.95–1.00$ or concentration of stresses caused by shape of the weld and welded part. Stresses σ_{eq} are calculated from the actual loads or by a conservative method from the $\sigma_{eq} \le 1.5[\sigma]$ condition.

With the simplified approach, where equivalent stresses are estimated by the conservative method from the $\sigma_{eq} \le 1.5[\sigma]$ condition, the resulting values of σ_{eq} are assumed to be identical for welded joints of

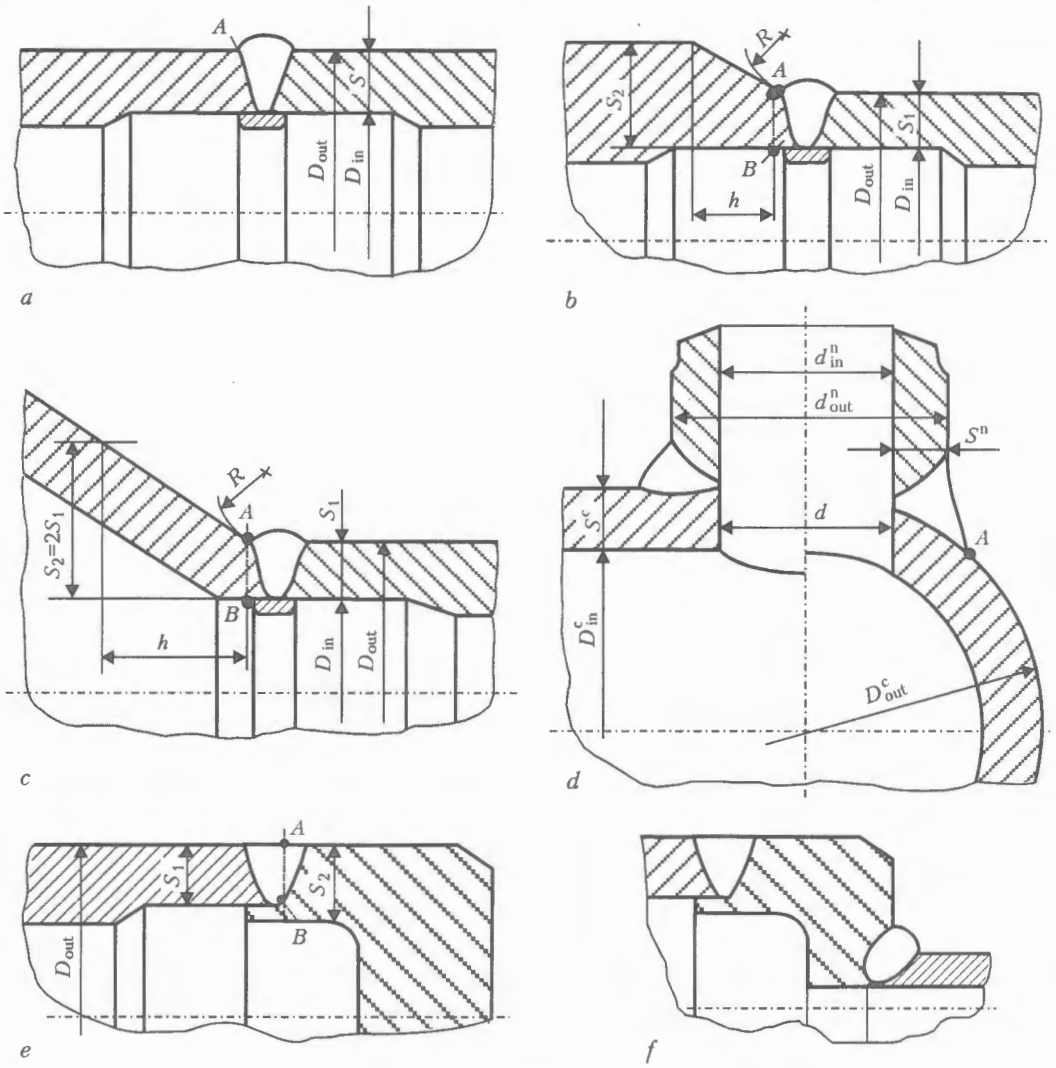

Figure 2. Calculation models of welded joints in steam pipelines [6]: *a* — butt welded joint between pipe elements with the same wall thickness (BWJ); *b*, *c* — butt welded joints between pipe elements of a different wall thickness ($BWJ_{d.t}$), including to a thick-wall branch pipe (*e*) and conical transition piece (*c*); *d* — T- (or nipple) welded joint (TWJ or NWJ); *e* — butt welded joint between pipe and bottom (BWJ_b); *f* — nipple welded joint between branch pipe and bottom (NWJ_b); *A*, *B* — points of maximal stresses

Table 1. Recommended periodicity and scopes of field inspection depending upon the safety factor for strength of welded joints in steam pipelines of Cr–Mo–V steels at $T \geq 510$ °C

HR	*Safety factor for strength*	*Periodicity of inspection of butt welded joints by MPI, USI and MAR methods, thous. h*		*Scope of inspection of welded joints (%) by methods*			
				MPI, USI		*MAR*	
		Type 1	*Type 2*	*Type 1*	*Type 2*	*Type 1*	*Type 2*
1	$n_d \geq 1.5$	50	50	20	100	0	10
2–3	$1.5 \geq n_d \geq 1.3$	40–50	20–30	20	100	10–15	20–30
4–5	$1.3 \geq n_d \geq 1.2$	30–40	15–20	40–50	100	20–25	40–50
6–7	$1.2 \geq n_d \geq 1.0$	20–30	10–15	100	100	40–50	100

Notes. 1. Scopes and periodicity of subsequent inspection should be refined proceeding from the results of verification calculations of strength based on actual sizes and types of welded joints and from the diagnostics results. 2. Inspection within the specified scope and with the specified periodicity should be done to welded joints of each size and type. Welded joints in regions of steam pipelines adjoining the boiler or located near the fixed supports or starting-regulating equipment, as well as joints in pipe elements with thinned walls and/or containing repair (backing) beads should be subjected to inspection within the specified scope and with the specified periodicity in the first place. 3. Type 1 — BWJ according to [6] (Figure 2, *a*); type 2 — $BWJ_{d.t}$ [6] (Figure 2, *b–f*); MPI — magnetic powder inspection; USI — ultrasonic inspection; MAR — metallographic analysis using replicas.

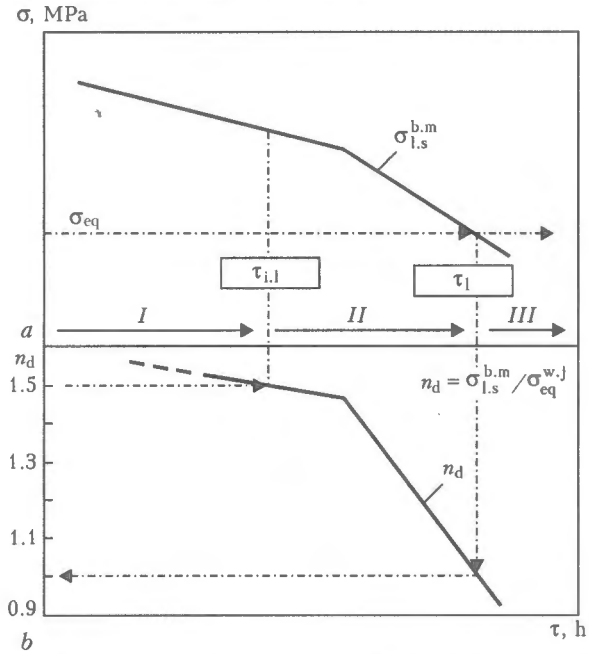

Figure 3. Diagram for determination of life (*a*) and safety factor for strength (*b*) of welded joints on the basis of rated durability of base metal $\sigma_{l.s}^{b.m}$ under creep conditions: τ_l — limiting life, thous. h, $n_d = 1$; $\tau_{i.l}$ — individual life, thous. h, $n_d \geq 1$; $\sigma_{eq}^{w.j}$ — calculated equivalent stresses due to all types of loads, allowing for φ_ω and $\varphi_{b\omega}$, MPa (φ_ω — safety factor for strength of welded joint with a transverse weld for tensile loading conditions; $\varphi_{b\omega}$ — same for bending loading conditions); *I* — period of reliable operation (condition $n_d \geq 1.5$ is met); *II* — period of possible further operation, $1 \leq n_d < 1.5$ (welded joints require more stringent inspection); *III* — period of risky (hazardous) operation

the same type in terms of design, size and steel grade of the parts used in a given steam pipeline. With the refined approach, stresses σ_{eq} are determined on the basis of actual loads evaluated from the results of examination of the support-overhead system and changes in shape and route of a steam pipeline. In this case the values of σ_{eq} will differ for welded joints

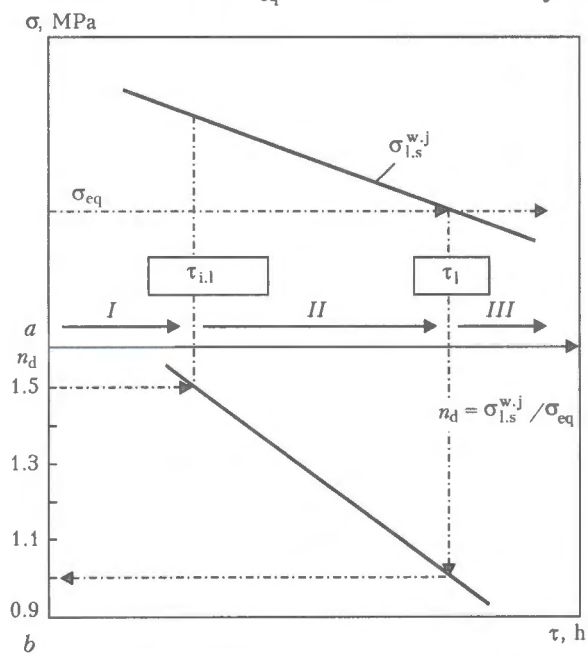

Figure 4. Diagram for determination of life (*a*) and safety factor for strength (*b*) of welded joints on the basis of their long-time strength $\sigma_{l.s}^{w.j}$ (σ_{eq} is calculated with no allowance for φ_ω and $\varphi_{b\omega}$)

of the same type, depending upon their location in the steam pipeline route and, accordingly, loading conditions in different regions of this route.

Residual life of welded joints is estimated on the basis of the following difference:

$$\tau_{r.l} = \tau_{i.l} - \tau_{o.l} \text{ (thous. h)},$$

where $\tau_{i.l}$ is the individual life (or limiting life τ_l for the safety factor for strength $n_d = 1$, Figures 3 and 4), which is determined from the results of comparison of long-time strength $\sigma_{l.s}$ and σ_{eq} of steel, allowing for the permissible acceptable values of n_d; and $\tau_{o.l}$ is the operating lifetime.

This is a typical version of solution of the problem. Here the safety factor for strength of welded joints is determined from the $n_d = \sigma_{l.s}/\sigma_{eq}$ relationship. The safety factor for strength is found from the diagrams shown in Figures 3 and 4, based on the periods of operating lifetime $n_{d.o.l}$ and residual life $n_{d.r.l}$, followed by evaluation of hazard rating (HR) of welded joints calculated from the linear dependence with boundary values HR = 1 (high-reliability welded joints) and HR = 7 (low-reliability welded joints), as derived by «VTI». The refined scopes and periodicity of subsequent field inspection of welded joints are assigned on the basis of the HR values thus found (Table 1).

When solving the problem on the basis of actual residual long-time strength of welded joints, residual life is found from the period of operating lifetime of a steam pipeline (period of cutting welded joints for testing) to that of limiting life τ_l, characterising the limiting state of metal, $n_d = 1$, i.e. residual life is estimated primarily from the $\tau_{r.l} = \tau_l - \tau_{o.l}$ relationship.

The following conclusions can be made from comparative analysis of the efficiency of these methods:

- method for determination of actual residual long-time strength of welded joints, involving the calculation of σ_{eq} from the actual loads, is most correct (and, at the same time, most labour-consuming and expensive) for estimation of $\tau_{r.l}$; this method is characterised by confidence factor CF ≥ 70 %;
- methods for determination of life on the basis of standardised rated values of long-time strength of steel, involving the calculation of σ_{eq} using the simplified approach, are less accurate (conservative in terms of safety factor for strength); at the same time, they are more cost-effective and less time-consuming (CF ≥ 20 %);
- method based on using the reference value of durability of welded joints, involving σ_{eq} estimated by the simplified approach (where the data on actual loads are not available), takes an intermediate position (CF ≥ 40 %).

Calculation-experimental method based on structural factor. This method is employed for express estimation of residual life of welded joints from the actual state of metal (microdamage) in zones with maximal stresses. For this purpose, structural strength of welded joints is estimated from the values of mar-

Table 2. Classification of welded joints in steam pipelines of steels 12Kh1MF and 15Kh1M1F by structural strength parameters and recommended scopes of their inspection by the MAR method

Type of welded joint (see Figure 2)	*Structural strength parameters (SSP)*	*SSP for groups*			*Inspection scope (%) for groups*			*Location of welded joint in steam pipeline route*
		1	*2*	*3*	*1*	*2*	*3*	
TWJ (NWJ)	$d_h/(D^c_{out} - 2S^c_a)$	>0.75	<0.75	<0.75	100	50	25	In any location (primarily in the region of bridges and starting-regulating equipment)
	S^c/S^c_0	1.0–1.2	1.3–1.5	≥1.6	100	50	25	
	S^n/S^n_0	1.0–1.2	1.3–1.5	≥1.6	100	50	25	
$BWJ_{d.t}$ (BWJ_b)	S/S_0	1.0–1.2	1.3–1.5	≥1.6	100	40	20	Same and near fixed supports
BWJ	S/S_0	1.0–1.2	1.3–1.5	≥1.6	100	20	10	Near fixed supports and at bridges in regions adjoining T-joints

Notes. 1. The first to be inspected are welded joints of group 1, and then of groups 2 and 3. 2. In addition, the first to be inspected are also welded joints with the following characteristics: repaired, having backing beads; joints with revealed heterogeneity of hardness in zones, $HB_{w.m}/HB_{b.m} < 1$; earlier estimated as having HR ≥ 3. 3. Designations: D^c_{out} – outside diameter of T-joint casing; S^c_a – actual wall thickness of T-joint casing in fillet weld zone determined by USI; S^c and S^n – nominal wall thickness of T-joint casing and nipple, respectively; S^c_0, S^n_0 and S_0 – calculated wall thickness of T-joint casing, nipple and pipe element in butt welded joints, respectively (determined in accordance with strength design standards); S – rated wall thickness of pipe elements; $HB_{w.m}$ and $HB_{b.m}$ – hardness of weld and base metals, respectively.

ginal wall thickness of pipe elements in weld locations, S/S_0 (S_0 is the calculated wall thickness according to [5]), relative equality of wall thickness of pipe elements in a welded joint, $\beta = D_{out}/D_{in}$ (D_{out} and D_{in} are the outside and inside diameters, respectively, of a pipe element in the weld location), and weakening of the T-joint casing due to a nipple hole, $d_h/(D^c_{out} - 2S^c_a)$ (d_h is the hole diameter, D^c_{out}, D^c_a are the outside diameter and actual wall thickness of the T-joint casing in fillet weld location determined by the USI method) to identify the inspection zones by the calculation method. Classification of welded joints by structural strength parameters (Table 2) and justification of the inspection zones are done by the method described in [4].

Metallographic analysis of zones identified for diagnostics is performed using replicas (on sections of metal or by using a portable microscope). The analysis results serve as the basis for evaluation of the extent of exhaustion of life (Table 3), and residual life is found with allowance for operating lifetime $\tau_{o.l}$, i.e. $\tau_{r.l} = \tau_l - \tau_{o.l}$. Limiting life τ_l is estimated from the $\tau_{o.l}/\tau_l$ ratio (extent of exhaustion of life) for a given welded joint. Estimation of residual life by this method is done in compliance with the branch guideline document developed by «VTI» [7].

This method is characterised by a high reliability. It allows for the integrated effect of different factors (technology, design and operation) on the actual state of metal, i.e. degradation of structure and properties

Table 3. Hazard rating and extent of exhaustion of life of welded joints depending upon microdamage of steam pipeline metal in creep

HR	*Type of metal damage acc. to [7]*	*Classification of metal damage acc. to [7]*		*Exhaustion of life $\tau_{o.l}/\tau_l$*		*Terms of the next inspection, thous. h*	
		Stage	*Step*	*Steel 12Kh1MF*	*Steel 15Kh1M1F*	*Type 1*	*Type 2*
1	–	Ip	–	≤ 0.50	≤ 0.60	Acc. to [6]	
2	Individual pores with density $\rho \le 100/mm^2$	IIp	–	0.50–0.60	0.60–0.75	40–50	20–25
3	Same, $\rho \le 250/mm^2$	IIIp	III.1p	0.61–0.70	0.68–0.75	15–20	10–15
4	Same, $\rho \le 1000/mm^2$		III.2p	0.70–0.76	0.75–0.80	10–15	7–10
5	Same, $\rho > 1000/mm^2$		III.3p	0.76–0.82	0.80–0.85	7–8	7–8
6	Chains of fine pores 1–2 μm in size	IVp	IV.1p	0.82–0.87	0.85–0.89	7–8	7–8
	Chains of coarser pores, coalesced pores and/or clusters of pores, microcracks		IV.2p	0.87–0.92	0.89–0.93	5–7	5–7
7	Micro- and macrocracks	Vp	V.1p V.2p	0.92–1.00	0.93–1.00	3–4	3–4

Note. HR is estimated as follows: safe (HR = 1), insignificantly deteriorated (HR = 2), of low hazard (HR = 3), of increased hazard (HR = 4), very hazardous (HR = 5), highly risky (HR = 6), critical (HR = 7), where the probability of fracture of welded joints exists. Repair can be assigned at HR = 3, repair is mandatory at HR = 4+6, immediate repair or re-welding of a joint should be done at HR = 7.

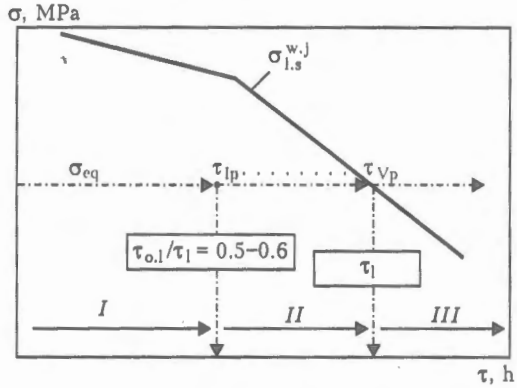

Figure 5. Schematic of the integrated approach to estimation of limiting life τ_l from long-time strength of welded joints, $\sigma_{l.s}^{w.j}$, followed by estimation of residual life $\tau_{r.l} = \tau_l = \tau_{o.l}$ from $\tau_{o.l}/\tau_l$ on the basis of structural factor; τ_{lp} — period estimated acc. to [7]; stages *I–III* — stages of reliable, possible and risky (hazardous) operation, respectively. Diagnostics acc. to [7] is required at stage *II*

in the form of micro- and up to macrodamage of the weakest regions of welded joints. In addition, this method is sufficiently fast and mobile. Normally, it is employed at heat power plants. However, its application involves certain labour expenditures associated with auxiliary and preparatory operations (grinding and polishing of inspection zones, removal and placement of heat insulation, installation of temporary scaffolding, etc.), as well as accuracy of selection of the inspection zones (without preliminary estimation of structural strength of welded joints from actual sizes of pipe elements in the weld locations).

Abroad, the scope of application of the MAR method for welded joints in steam pipelines of heat power plants is 50–100 % [4].

Integrated use of calculation-experimental methods based on long-time strength and structural factor (see Figure 1). This approach provides the most accurate results of estimation of residual life of welded joints. With this approach, the method based on long-time strength is considered to be of a primary importance and imperative for determination of general performance of welded joints for a period of operating lifetime (estimation of individual and residual life, safety factor for strength and HR, assignment of inspection). In this case the results of the calculation-experimental studies cover similar (in steel grade, design and size) welded joints, independently of their location in the steam pipeline route, whereas in estimation of σ_{eq} from actual loads the account is made of the location of joints in the steam pipeline route.

The method for estimation of residual life from the structural factor makes it possible to determine $\tau_{r.l}$ and HR of the joints allowing for their actual loading, proceeding from the location in the steam pipeline route. In this case, the first to be diagnosed are welded joints that cause doubts in terms of the results of the previous calculation-experimental studies.

Here the confirmation is a comparative estimation of $\tau_{r.l}$ and HR of welded joints in a steam pipeline, such as that made for a pilot power unit with a capacity of 300 MW at station No.5 of the Kostroma hydroelectric plant. The estimation was made on the basis of the results of the calculation-experimental studies conducted by «VTI» (Table 4). Thus, as determined by the calculation-experimental method on the basis of long-time strength of metal, for TWJ the residual life was classified as exhausted, i.e. $\tau_{r.l1} = 0$ and $HR_1 = 7$, independently of the location of TWJ in the steam pipeline route. Then, the residual life was estimated, checked and characterised by the results of subsequent diagnostics of TWJ and calculation-experimental studies on the basis of structural factor for each type of the welded joints as $\tau_{r.l2} =$ = 14,000–123,000 h with $HR_2 = 1.0–6.1$. Operations on estimation of these parameters for other dimensions and types of BWJ and $BWJ_{d.t}$ (Table 4) were carried out in a similar way.

Another example is the integrated approach developed by «VTI» for evaluation of residual life from the reference durability of welded joints, combined with the method of diagnostics using replicas. Limiting life τ_l is estimated at the first stage from long-time strength of welded joints on the basis of the calculation-experimental studies. Then the values of residual life are checked on the basis of structural factor (Figure 5). Period τ_{Ip} is found from [7]. Diagnostics by the MAR method is assigned starting from this period to check residual life of welded joints.

«VTI» performs contract works on evaluation of life of welded joints in steam pipelines by developing schedules of inspections for many heat power stations, including the Kostroma, Ryazan and Novocherkassk hydroelectric power stations, as well as Surgut hydroelectric power station 2, Novogorkovsk heat and power plant, etc.

Table 4. Comparative values of $\tau_{r.l}$ and HR found by the calculation-experimental methods for welded joints in steam pipeline of a pilot unit of steel 15Kh1M1F (operating life is 185,000 h at a temperature of 545 °C and pressure of 25.5 MPa)

Type of welded joint (see Figure 2)	D_{out}×S, *mm*	*Residual life, thous. h*		HR_1	HR_2	*Number of welded joint in steam pipeline diagram*
		$\tau_{r.l1}$	$\tau_{r.l2}$			
BWJ	325×60	215	>123	1	1	15, 18, 4
	325×60	215	79	1	2.1	7
$BWJ_{d.t}$	325×60 + + D_n200	50	>123	4	1	70, 71
TWJ	325×60 245×45	0	>123	7	1	76a, 78a
		0	79	7	2.1	77a
		0	43	7	4	68a
		0	14	7	6.1	31a, 75a

Notes. 1. $\tau_{r.l1}$ and HR_1 were found by the calculation-experimental method on the basis of long-time strength of metal; $\tau_{r.l2}$ and HR_2 were determined by the calculation method on the basis of structural factor (microdamage) of metal. 2. Welded joints BWJ belong to type 1, and $BWJ_{d.t}$ and TWJ belong to type 2, acc. to [6]. 3. Pipe elements of $BWJ_{d.t}$ are made from steel 15Kh1M1FL.

As shown by the results of the integrated calculation-experimental studies, allowing for the gained operating experience and results of statistical analysis of the inspection data and data on damageability, the residual life of welded joints in steam pipelines of power units with a capacity of 300 MW and lower, after operation for 100,000 h at a temperature of 545 °C, is characterised by the following values: 150,000–300,000 h for BWJ, 50,000–200,000 h for $BWJ_{d.t}$, and 50,000–100,000 h for TWJ (see Figure 2).

Welded joints in steam pipelines of power units with a capacity of 800 MW have a shorter residual life.

1. Khromchenko, F.A., Lappa, V.A., Kalugin, R.N. (2001) Diagnostics and service life of welded joints in steam pipelines of heat power plants. Part 2. *Svarochn. Proizvodstvo*, **8**, 21–24; Part 3. *Ibid.*, **9**, 15–19.
2. Khromchenko, F.A., Fedoseenko, A.V., Lappa, V.A. (1995) Evaluation of residual life of durable welded joints steam pipelines. *Teploenergetika*, **4**, 12–16.
3. Khromchenko, F.A., Lappa, V.A., Kalugin, R.N. (2001) Diagnostics and prediction of life of welded joints in steam pipelines. *Elektrich. Stantsii*, **7**, 55–62.
4. Khromchenko, F.A. (2002) *Life of welded joints in steam pipelines*. Moscow: Mashinostroenie.
5. (1999) *RD 10-249–98*. Standards for strength design of stationary boilers and steam and water pipelines. Moscow: NPO TsKTI.
6. (1999) *RD 10-262–98* (RD 153-34.1-17.421–98). General instructions for inspection of metal and extension of service life of main elements of heat power plant boilers, turbines and pipelines. Moscow: ORGRES.
7. *RD 153-34.1-17.467–2001*. Express method for evaluation of residual life of welded joints in boiler collectors and steam pipelines on the basis of structural factor. Moscow: VTI.

COMPARATIVE ANALYSIS OF LASER, PLASMA AND COMBINED METHODS FOR HEATING FINELY DISPERSED CERAMIC PARTICLES

A.I. BUSHMA, A.T. ZELNICHENKO and **I.V. KRIVTSUN**
E.O. Paton Electric Welding Institute, NASU, Kiev, Ukraine

Temperature fields in finely dispersed ceramic particles (Al_2O_3 and SiO_2) heated by the CO_2-laser radiation, argon plasma flow and their combination, using volume, surface and combined heat sources, have been calculated through solving the non-stationary equation of heat conduction for a spherical particle, allowing for dependence of optical and thermal-physical properties of particle materials upon the temperature. Shown is the effect on space-time distribution of temperature of the above particles by a heating method, as well as optical and thermal-physical properties of the materials.

Keywords: *laser radiation, plasma flow, finely dispersed ceramic particles, heat source, temperature field, combined laser-plasma heating*

Along with the known technologies for thermal spraying of coating, such as plasma spraying [1], the processes of laser spraying based on adding powder particles to the laser beam, heating (melting) and depositing them on the substrate material surface [2] are finding currently an increasingly wide application. The fundamental difference between these processes lies in different mechanisms of heating of finely dispersed materials. In one case the spray particles are heated by a flow of hot air or plasma (surface heat source), and in the other case the particles are heated by absorbing laser radiation. It should be noted that in the case of heating metallic particles by the CO_2-laser radiation the heat released is concentrated in a very thin subsurface layer of their material [3], i.e. here the heat source can also be considered to the surface type. The situation with laser heating of finely dispersed dielectric, e.g. ceramic, particles is substantially different. In contrast to metals, most ceramic materials are sufficiently transparent to the CO_2-laser radiation with wavelength $\lambda = 10.6$ μm, and at $d/\lambda \cong \cong 1$ (where d is the particle size) they absorb its energy in the entire volume of a particle [4]. In this case the heat source is of the volume type. Moreover, in some instances it may be concentrated near the particle centre [3, 4].

Therefore, the processes of plasma and laser spraying of finely dispersed ceramic materials may differ greatly not only in integrated characteristics of a heat source determining the particle heating rate, but, more importantly, also in distributed characteristics of the heat released in spray particles. As ceramic materials are characterised by a relatively low thermal conductivity, temperature fields in ceramic particles may be rather heterogeneous across a particle and greatly depend upon the method used to heat it. In view of the above-said, the objective of this study was to investigate peculiarities of laser, plasma and combined (laser-plasma) heating of finely dispersed ceramic particles.

Consider the above peculiarities by an example of spherical Al_2O_3 and SiO_2 particles, assuming that radius of a particle is commensurable with the laser radiation wavelength. As non-uniformity of heating of such particles may lead to a substantial non-uni-

formity of distribution of optical and thermal-physical properties of a particle material depending upon the temperature, hereinafter we will consider the particles to be radially heterogeneous.

Distributed and integrated characteristics of absorption of laser radiation by the particles under consideration can be determined by using the approach suggested in [4]. Let a plane electromagnetic wave fall on a particle with radius a in a direction of axis Oz of the spherical coordinate system (r, φ, ϑ) with an origin at the particle centre. The electromagnetic energy absorbed per unit time in a unit volume of the particle can be determined from the known relationship [5]:

$$D = -\text{div } \mathbf{S},$$

where $\mathbf{S}(r, \varphi, \vartheta)$ is the time (for a wave field oscillation period) averaged value of the Pointing vector of the electromagnetic field induced in the particle by incident radiation. Assuming that the particle rotates about its own axis normal to axis Oz, and considering that the initial laser radiation is non-polarised, it is possible to replace $D(r, \varphi, \vartheta)$ by the angle averaged power released in a unit volume of the particle material:

$$D(r) = -\frac{1}{4\pi}\int_0^{2\pi} d\varphi \int_0^{\pi} \sin\vartheta \frac{1}{r^2}\frac{\partial}{\partial r}[r^2 S_r(r, \varphi, \vartheta)]d\vartheta.$$

If a period of complete revolution of the particle is much shorter than the characteristic time of change in its temperature, the thermal field of this particle can be considered spherically symmetric, and heterogeneity of its dielectric permittivity can be considered substantial only in a radial direction.

Use the method of layered approximation [6] to find fields induced by the electromagnetic wave in a radially heterogeneous spherical particle having complex dielectric permittivity $\varepsilon(r)$ and determine an explicit form of the $D(r)$ value. Divide conditionally the particle into N spherical layers and assume that dielectric permittivity of its material, ε, is constant within each layer:

$$\varepsilon(r) = \varepsilon_l \equiv \varepsilon_l' + i\varepsilon_l''; \quad a_{l-1} < r \le a_l \ (l = 1, 2, \ldots, N),$$

where ε_l' and ε_l'' are the real and imaginary parts of dielectric permittivity, respectively; and a_l and a_{l-1} are the outer and inner radii of the l-th layer ($a_0 = 0$, $a_N = a$). It is obvious that by increasing the number of layers we can achieve an arbitrarily accurate approximation of optical properties of a non-uniformly heated particle. It should be noted that this method also allows determination of distribution of the absorbed power in layered particles consisting of different materials.

Using an analytical solution of the problem of the layered-heterogeneous sphere diffraction of a plane wave [7], we find that

$$D(r) = \frac{S^{\text{inc}}\varepsilon_l''}{8k}\sum_{m=1}^{\infty}(2m+1)\sum_{\gamma=1,2}\times$$
$$\times\left\{|\, d_\gamma^{(l)}\,|^2 F_\gamma^{(l)}(r) + 2\text{Re}\left[d_\gamma^{(l)}\tilde{d}_\gamma^{(l)*} H_\gamma^{(l)}(r)\right] + |\,\tilde{d}_\gamma^{(l)}\,|^2 G_\gamma^{(l)}(r)\right\}, \quad (1)$$
$$a_{l-1} < r \le a_l \ \ (l = 1, 2, \ldots, N).$$

Here S^{inc} is the intensity of an incident laser radiation falling on the particle; $k = 2\pi/\lambda$ is its wave vector; functions $F_{1,2}^{(l)}(r)$, $H_{1,2}^{(l)}(r)$ and $G_{1,2}^{(l)}(r)$, as well as values $d_{1,2}^{(l)}$ and $\tilde{d}_{1,2}^{(l)}$, are given in study [4]. Here the asterisk marks the complex conjugate value.

Solution of the diffraction problem [7] allows finding the full sections of absorption Q^d and dissipation Q^s of electromagnetic waves by a radially heterogeneous spherical particle, along with the $D(r)$ value. The final result of the calculations can be represented as follows:

$$Q^e = -\frac{\pi}{k^2}\sum_{m=1}^{\infty}(2m+1)\sum_{\gamma=1,2}\text{Re}(q_\gamma),$$
$$Q^s = \frac{\pi}{2k^2}\sum_{m=1}^{\infty}(2m+1)\sum_{\gamma=1,2}|\, q_\gamma\,|^2,$$

where $Q^e = Q^d + Q^s$ is the extinction section [8], and the values of $q_{1,2}$ were taken from [4]. Figure 1 shows the results of calculations of radial distributions of the CO_2-laser radiation power absorbed by the homogeneous spherical Al_2O_3 and SiO_2 particles of a differing diameter (optical constants of the above dielectric materials for radiation with $\lambda = 10.6$ μm were taken from [9]). With the Al_2O_3 particles the laser radiation power dissipated in a unit volume of a spherical particle decreases in a direction from its surface to the centre, the non-uniformity of heating growing with increase in the a values (compare curves *1* and *2* in Figure 1, *a*). The SiO_2 particles are characterised by an opposite situation. Maximum of the $D(r)$ dependence formed inside a particle decreases with increase in its radius (Figure 1, *b*). As a result, heating of the SiO_2 particles by the CO_2-laser radiation occurs more uniformly with increase in the particle radius. Full radiation power Q^l absorbed by the particles considered can be determined as a product of the corresponding absorption section by the intensity of incident laser radiation falling on a particle. At $S^{\text{inc}} = 1 \cdot 10^9$ W/m^2, this yields $Q^l = 0.92$ W for the Al_2O_3 particles and $Q^l = 2.3$ W for the SiO_2 particles. Radius of the particles in both cases was 30 μm.

For the case of plasma heating of spherical particles, we will use a combined model of convection-radiation heat transfer [10] to describe the exchange of energy between the plasma flow and a particle. According to this model, the heat flow through the particle surface can be written down as follows:

$$q = \alpha(T_p - T_s) + \xi\sigma_0(T_p^4 - T_s^4), \quad (2)$$

where α is the heat transfer coefficient; T_p is the temperature of the non-disturbed plasma flow falling

on the particle; T_s is the particle surface temperature; ξ is the reduced emissitivity factor for the plasma–particle surface system; and σ_0 is the Stefan–Boltzmann constant. The convective heat transfer coefficient for a spherical particle can be calculated from the criterial dependence for a flow about a sphere [11]:

$$\mathrm{Nu} = 2\frac{\chi_s}{\chi_p} + 0.5\mathrm{Re}^{0.5}\mathrm{Pr}^{0.4}\left(\frac{\rho_p\eta_p}{\rho_s\eta_s}\right)^{0.2}. \quad (3)$$

Here $\mathrm{Nu} = (\alpha 2a)/\chi_p$ is the Nusselt number; $\mathrm{Re} = (\rho_p u_p 2a)/\eta_p$ is the Reynolds number; $\mathrm{Pr} = (C_p\eta_p)/\chi_p$ is the Prandtl number; χ_p is the coefficient of thermal conductivity of the non-disturbed plasma; ρ_p is its density; C_p is the dynamic viscosity factor; η_p is the specific heat (index s designates corresponding properties of the plasma at temperature of the particle surface); and u_p is the velocity of the plasma flow with respect to the particle. For example, when the particles considered are flown about by the argon plasma under the atmospheric pressure at temperature $T_p = 8000$ K and velocity $u_p = 150$ m/s, the heat flow through the surface of the particle with radius 30 μm, as calculated according to (2) and (3), is $q = 2.0\cdot10^8$ W/m^2 (the full power input to the particle is $Q^p = 2.3$ W) for the Al_2O_3 particles and $q = 1.2\cdot10^8$ W/m^2 ($Q^p = 1.4$ W) for the SiO_2 particles, having a temperature of 300 K (the data on the required thermal-physical properties and transfer coefficients for the argon plasma were taken from [12]).

Allowing for the probable non-uniformity of a space distribution of temperature, to calculate temperature fields in ceramic particles heated by laser radiation, plasma flow or their combination, in a general case we will use the non-stationary equation of heat conduction with a distributed heat source. Assuming a spherical symmetry of the temperature field of a particle and dependence of its material properties upon the temperature, this equation can be written down as follows:

$$\rho\overline{C}\frac{\partial T}{\partial t} = \frac{1}{r^2}\frac{\partial}{\partial r}\left(r^2\chi\frac{\partial T}{\partial t}\right) + D(r, t), \quad 0 \le r \le a(t). \quad (4)$$

Here $\rho(T)$ is the density of the particle material; $\overline{C}(T)$ is its effective heat capacity calculated with allowance for the latent heat of melting W_M and vapour formation W_B; $T(r, t)$ is the space-time distribution of temperature in the particle; $\chi(T)$ is the thermal conductivity coefficient; $a(t)$ is the current value of its radius; and

$$\overline{C} = c + W_M\,\delta(T - T_M) + W_B\,\delta(T - T_B),$$

where $c(T)$ is the specific heat of the material; T_M and T_B are the melting and boiling temperatures, respectively; and $\delta(x)$ is the delta function. The $D(r, t)$ value describing the energy released in the bulk of a particle in the case of laser and combined heating can be calculated from (1), allowing for time variations of both space distribution $\varepsilon[T(r, t)]$, associated with non-uniform heating of the particle, and radius

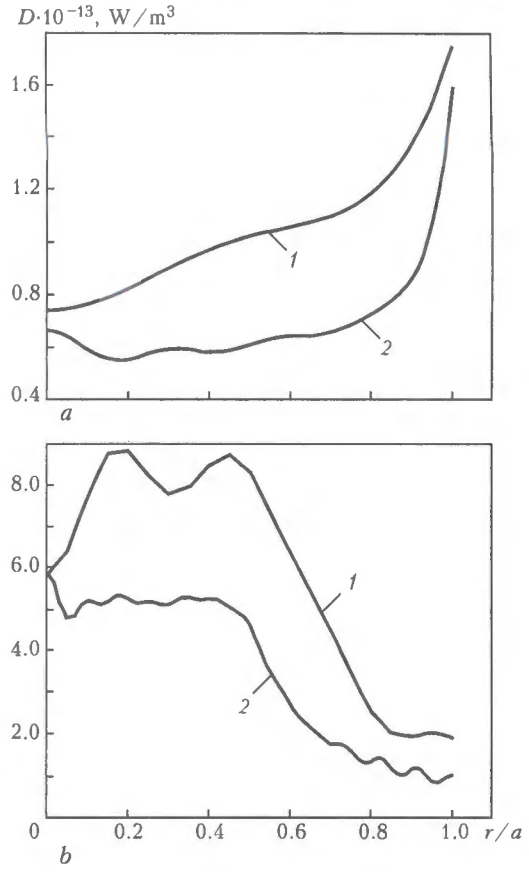

Figure 1. Radial distributions of power of the CO_2-laser radiation absorbed by homogeneous spherical Al_2O_3 (*a*) and SiO_2 (*b*) particles at $S^{inc} = 1\cdot10^9$ W/m^2: *a* — $\varepsilon' = 0.490$, $\varepsilon'' = 0.028$; *b* — $\varepsilon' = 4.750$, $\varepsilon'' = 0.096$; *1* — $a = 10$; *2* — 30 μm

of this particle, e.g. in evaporation. In modelling of plasma heating of the particle, the volume heat source in equation (4) is assumed to be equal to zero.

Initial and boundary conditions for equation (4) can be written down as follows:

$$T(r)\,|_{t=0} = T^0,\ a\,|_{t=0} = a^0;\ -\left(\chi\frac{\partial T}{\partial r}\right)|_{r=a} = q,\ \frac{\partial T}{\partial r}|_{r=0} = 0,$$

where T^0 and a^0 are the initial values of temperature and radius of the particle, respectively. In the case of plasma and combined heating, the value of q is calculated from (2) and (3). In modelling of laser heating, it is assumed that the particle heated is in the flow of a cold gas, having temperature T_{ext} and relative velocity u_{ext}. In this case the heat transfer from its surface can also be described by relationships (2) and (3), assuming in them that $T_p = T_{ext}$ and $u_p = u_{ext}$.

The fully implicit difference scheme with time splitting of steps, providing a complete allowance for the latent heat of melting and vapour formation, was used to find numerical solution to equation (4). It was assumed that the evaporated material would immediately leave the particle surface, causing no attenuation of the incident radiation flow falling on it, and exerting no effect on the conditions of heat transfer between the particle and environment.

Figure 2 shows variations with time t of the calculated values of temperature at the centre, T_c, and

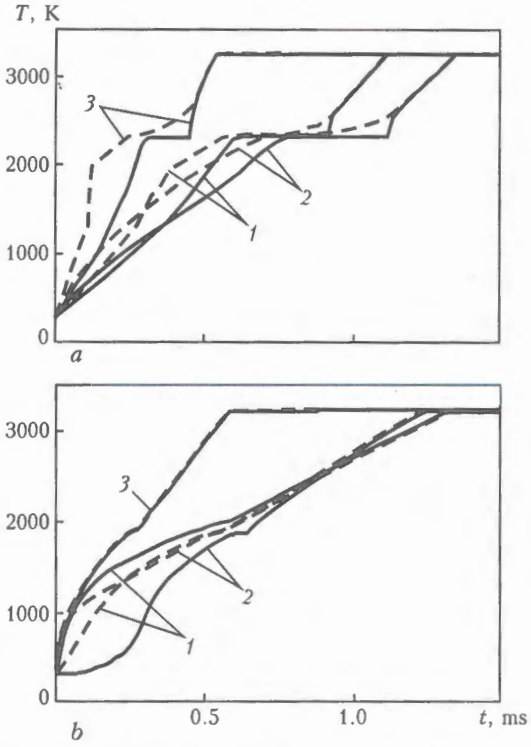

Figure 2. Time dependencies of temperature at the centre (*solid curves*) and on the surface (*dashed curves*) of spherical Al_2O_3 (*a*) and SiO_2 (*b*) particles with radius a = 30 μm heated by CO_2-laser radiation (*1*), argon plasma flow (*2*) and their combination (*3*) at a velocity of the flow about the particles equal to u_p = 150 m/s: *1* – $S^{inc} = 10^9$ W/m^2, T_p = 300 K; *2* – S^{inc} = 0, T_p = 8000 K; *3* – $S^{inc} = 10^9$ W/m^2, T_p = 8000 K

on the surface, T_s, of the Al_2O_3 and SiO_2 particles during heating by the CO_2-laser radiation, argon plasma flow and their combination (required temperature dependencies of thermal-physical parameters and optical properties of the materials considered were taken from [4]). As follows from Figure 2, the non-uniform distribution of a volume heat source in particles heated by laser radiation (see Figure 1) leads to the fact that temperature on the Al_2O_3 particle surface at the initial stages of heating grows faster than at the particle centre (compare dashed and solid curves *1* in Figure 2, *a*), whereas in the case of SiO_2 we see the opposite situation (see Figure 2, *b*). In plasma (surface) heating of the particles, temperature on the surface of a particle grows faster than at its centre for both materials (curves *2* in Figure 2). As far as the combined heating method is concerned, here the non-uniformity of heating markedly grows for the Al_2O_3 particles (curves *3* in Figure 2, *a*), and substantially decreases for the SiO_2 particles (curves *3* in Figure 2, *b*). As a result, combined heating of the SiO_2 particles may be almost uniform.

Therefore, the conducted numerical analysis of different methods used to heat finely dispersed ceramic materials under spraying conditions allows a conclusion that the space-time distribution of temperature in spray particles can be controlled by employing the certain combination of plasma (surface) and laser (volume) heating. This combination of the heating methods is implemented in a new process, i.e. hybrid plasma-laser spraying.

1. Petrov, S.V., Karp, I.N. (1993) *Plasma air-gas spraying*. Kiev: Naukova Dumka.
2. Pawlowski, L. (1999) Thick laser coatings. A review. *J. Thermal Spray Technol.*, 8(2), 279–295.
3. Bushma, A.I., Krivtsun, I.V. (2003) Peculiarities of absorption and scattering of different wavelength laser radiation by fine spherical particles. In: *Proc. of Int. Conf. on Laser Technologies in Welding and Materials Processing*, Katsiveli, Crimea, Ukraine. Kiev: PWI.
4. Bushma, A.I., Krivtsun, I.V. (1992) Peculiarities of heating of fine ceramic particles by laser radiation. *Fizika i Khimiya Obrab. Materialov*, 2, 40–48.
5. Landau, L.D., Lifshits, E.M. (1982) *Electrodynamics of continua*. Moscow: Nauka.
6. Brekhovskikh, L.M. (1973) *Waves in layered media*. Moscow: Nauka.
7. Gvozdetsky, V.S., Zagorodny, A.G., Krivtsun, I.V. et al. (1983) *Radiation of heterogeneous plasma sphere*. Preprint. Kiev: ITF.
8. Born, M., Volf, E. (1968) *Principles of optics*. Moscow: Nauka.
9. Zolotoryov, V.M., Morozov, V.N., Smirnova, E.V. (1984) *Optical constants of natural and technical media*. Refer. Book. Leningrad: Khimiya.
10. Kutateladze, S.S. (1979) *Principles of heat exchange theory*. Moscow: Atomizdat.
11. Tsvetkov, Yu.V., Panfilov, S.A. (1980) *Low-temperature plasma in repair processes*. Moscow: Nauka.
12. Boulos, M.I., Fauchais, P., Pfender, E. (1997) *Thermal plasmas: Fundamentals and applications*. Vol. 1. New York-London: Plenum Press.

DISTRIBUTION OF TEMPERATURE IN AIR JET AND SUBSTRATE DURING ELECTRIC ARC METALLISING

N.M. VOROPAJ[1], A.I. MAZHEJKA[2] and S.I. MARKOVICH[2]
[1]E.O. Paton Electric Welding Institute, NASU, Kiev, Ukraine
[2]Kirovograd State Technical University, Kirovograd, Ukraine

Effect of the electric arc metallising process parameters on distribution of temperature in air jet and substrate is considered. The method for measurement of temperature in individual regions of the jet and substrate with variations in the arc current, air pressure and spraying distance is used. It is shown that temperature of the jet and substrate increases with increase in the arc current and air pressure.

Keywords: *electric arc metallising, process parameters, electrode wire, air jet, jet temperature, substrate temperature, coating thickness*

Quality of formation of coatings in electric arc metallising greatly depends upon the axial and radial distribution of temperature in air jet and thermal conditions at the interface between the molten particles of a spray material and surface of the base metal (substrate) [1–3]. The energy source in electric arc metallising is the electric arc burning between two consumable electrodes in a compressed air jet. Main parameters of this process are arc current I_a, arc voltage U_a, compressed air pressure P and spraying distance L_s.

The studies [4] were earlier conducted to investigate the effect of some parameters of the plasma spraying process on temperature of the jet of argon and its mixture with hydrogen. In this study the authors used the method of sounding some regions of the electric arc metallising zone to determine the distribution of temperature in air jet and substrate with variations in the process parameters.

The experiments were conducted using the electric arc spraying machine KDM-4 [5] consisting of the metallising unit EM-14M with a central nozzle-type system for feeding the compressed air, DC power supply of the VS-632 type with a quietly drooping characteristic, and a movable table to move the samples being sprayed. The use was made of two electrode wires: flux-cored wire NPP-5 with a core of the Fe–C–Cr–Mn system (cathode) and all-drawn wire of the Sv-08A grade (anode) (0.08 wt.% C). Diameter of the wires was 2 mm, and their feed speed was 360–540 m/h. Like in study [4], temperature in the air jet was measured using the chromel-alumel thermocouples with a diameter of 0.5 mm. The maximal width of the welded end of a thermocouple was 1.2 mm. To avoid hitting the thermocouples by metal drops, their working regions were insulated by a heat-resistant ceramic tube with an outside diameter of 4 mm. Temperature of the fixed substrate was measured with the chromel-copel thermocouples with a diameter of 0.2 mm. The steel 09G2 (wt.%: 0.09C; 2.0Mn; Fe – balance) substrate samples measuring 200×200 mm and 3 mm thick were made with upper holes 1.5 mm deep. The thermocouples were welded into the holes using a capacitor-discharge welding device. The thermoelectric effect induced by the thermocouples immersed into the air jet and substrate was registered using an oscilloscope.

The most typical parameters of spraying used in the experiments are given in the Table. Distance from the nozzle exit section to the point of measurement of the jet temperature was 30–90 mm. The arc current was varied from 150 to 250 A at U_a = 24–28 V. The compressed air pressure was 0.1, 0.3 and 0.4 MPa. The selected spraying distance ranged from 100 to 200 mm. During the experiments the thermocouples were installed along the axis of the air jet and substrate at a distance of 10, 20 and 40 mm from the axis.

Temperature of the air jet grows with increase in the arc current in all the modes of the electric arc

Parameters of the electric arc metallising process

Mode number	*Arc current I_w, A*	*Arc voltage U_a, V*	*Air pressure P, MPa*	*Spraying distance L_s, mm*	*Distance from nozzle to temperature measurement point L_n, mm*
1	150	24	0.1	150	30
2	150	24	0.3	150	30
3	150	24	0.4	150	30
4	250	28	0.1	150	30
5	250	28	0.3	150	30
6	250	28	0.4	150	30
7	150	24	0.3	150	60
8	150	24	0.3	150	90
9	250	28	0.3	150	60
10	250	28	0.3	100	90
11	150	24	0.3	100	60
12	250	28	0.3	100	60
13	150	24	0.3	200	60
14	250	28	0.3	200	60

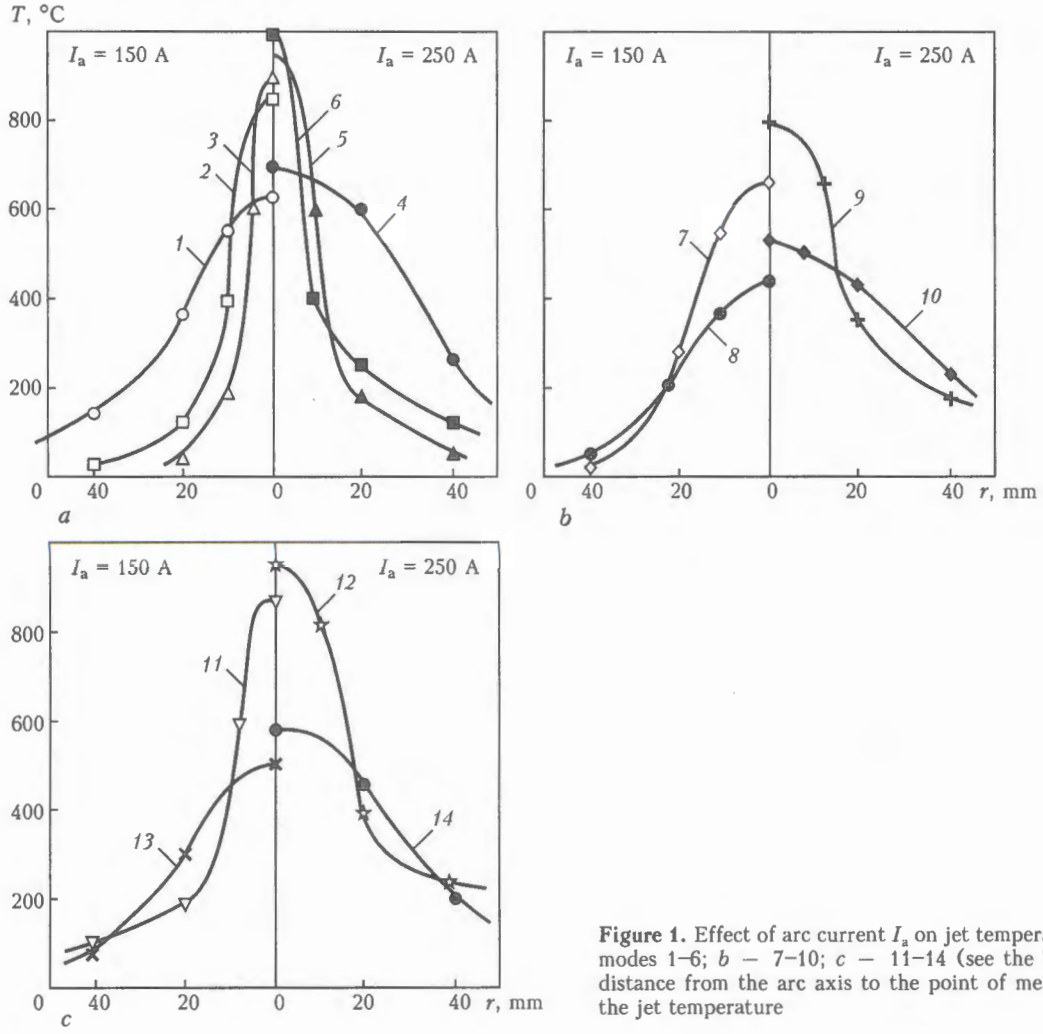

Figure 1. Effect of arc current I_a on jet temperature T: *a* — modes 1–6; *b* — 7–10; *c* — 11–14 (see the Table); r — distance from the arc axis to the point of measurement of the jet temperature

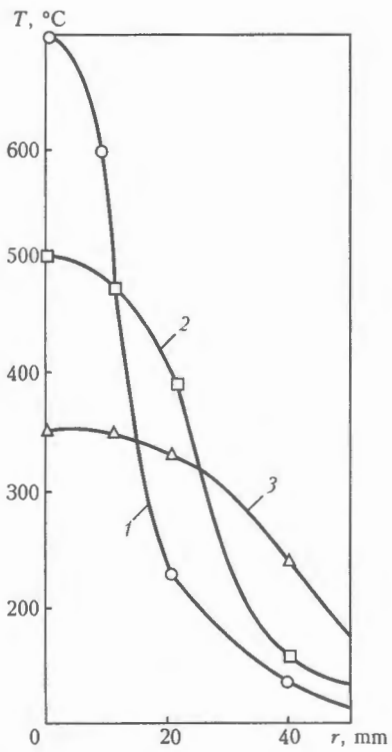

Figure 2. Effect of spraying distance on distribution of temperature in metal substrate at I_a = 200 A, U_a = 26 V, P = 0.4 MPa and t = = 6 s: *1* — L_s = 100; *2* — 150; *3* — 200 mm

metallising process (Figure 1). Air pressure also affects the jet temperature. For instance, at P = 0.1 MPa and I_a = 150 A the maximal temperature of the jet at the axis is somewhat higher than 600 °C. Diameter of the jet, having a temperature of 400 °C, amounted to 40 mm at I_a = 150 A and 60 mm at I_a = 250 A. As the air pressure is increased to 0.4 MPa, temperature of the jet at its axis grows to 900 °C at I_a = 150 A and 1000 °C at I_a = 250 A. With such an increase in the air pressure the high-temperature region of the jet decreases 3–4 times.

The distribution of temperature in metal substrate as a function of spraying distance L_s is shown in Figure 2. At a relatively small (100 mm) spraying distance the substrate temperature amounts to 700 °C and continues growing with decrease in L_s. At a spraying distance of 150–200 mm the substrate temperature decreases to 350–500 °C, which leads to increase in the heating zone temperature to 300 °C. Thickness of a coating within the heating spot varies in a similar way: the higher the arc current and spraying time, the thicker the coating at the heating spot centre (Figure 3).

For the given diameter of the electrode wires (2 mm) the optimal values of the arc current and arc voltage in electric arc metallising are 250 A and 28 V, respectively. At lower values of the arc current (100–

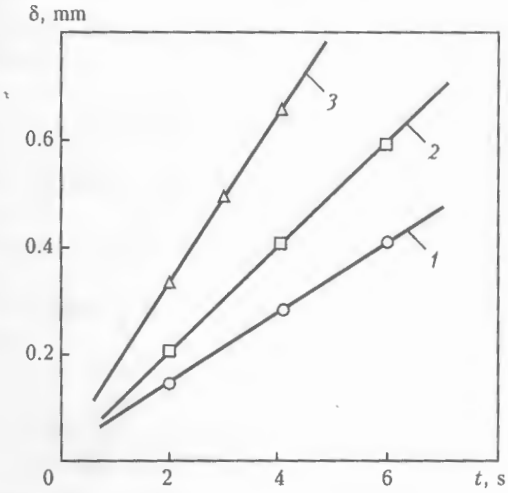

Figure 3. Effect of spraying time t on coating thickness δ at the heating spot centre at different values of the arc current: *1* — I_a = = 100; *2* — 150; *3* — 200 A

150 A) there is a decrease in the productivity of the spraying process. In this case the coating to substrate adhesion strength is relatively low. As the current is increased to 350 A and more, the length and diameter of the arc plume grow. This is accompanied by increase in the extent of spattering of the electrode metal and oxidation of the sprayed material surface.

Quality of the sprayed coating greatly depends also upon the air pressure and spraying distance. At low values of the air pressure (0.1–0.2 MPa) the resulting coatings have a coarse-grained metal structure (Figure 4, *a*). Increase in the air pressure to 0.4 MPa leads to decrease in grain size (Figure 4, *b*). In both cases the matrix phase in metal structure of a coating is solid solution of chromium in α- or γ-iron. A carbide phase is formed in structure of the coating, leading to a marked increase in its hardness [3]. At a spraying distance of up to 150 mm, the molten electrode metal particles reach the substrate surface, thus providing dense coatings characterised by a strong adhesion to the substrate. At a spraying distance of more than 200 mm the spray material particles may be overcooled, and the coating to base metal adhesion strength may decrease. Specific parameters of the electric arc metallising process are required for each dimension and type of a part sprayed. A small amount of easily ionised compounds of alkali or alkali-earth metals should be added to a flux-cored wire to increase stability of the arc [6]. Such additions allow the electric arc metallising process to be carried out at an alternating current and with a pulsed arc.

CONCLUSIONS

1. Temperature of the air jet in electric arc metallising increases with increase in the arc current and air pressure. The jet temperature along the axis decreases from 900–1000 to 500–600 °C with increase in the spraying distance from 100 to 200 mm. The high-temperature region of the jet decreases 3–4 times almost along its entire length with the air pressure increased to 0.4 MPa. The closer to the nozzle, the more dramatic is the temperature gradient in peripheral layers of the jet under all conditions considered.

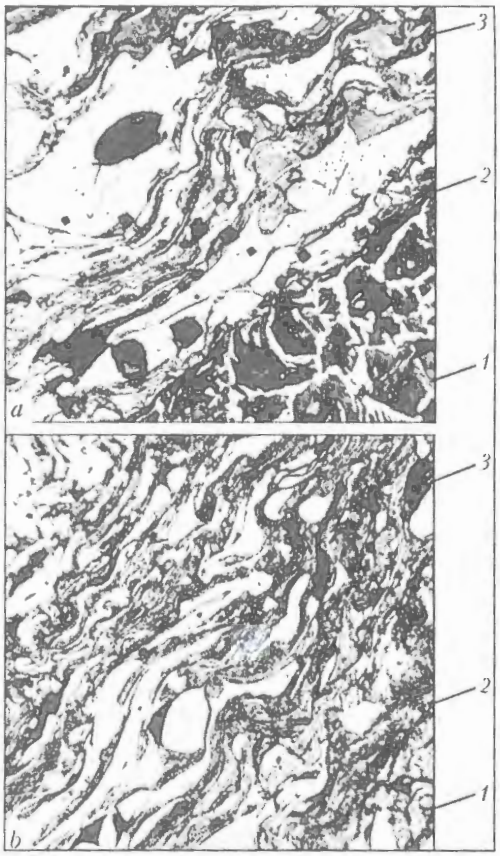

Figure 4. Microstructure of coating sprayed using the flux-cored and all-drawn wire at P = 0.1 (*a*) and 0.4 (*b*) MPa: *1* — substrate; *2* — interface; *3* — coating (×200)

2. As the spraying distance is increased from 100 to 200 mm, the temperature of the steel 09G2 substrate 3 mm thick decreases from 700 to 350 °C. The largest thickness of a coating on the substrate is along the heating spot axis. The higher the arc current and the longer the spraying time, the larger the coating thickness.

1. Borisov, Yu.S., Kharlamov, B.A., Sidorenko, S.A. et al. (1987) *Thermal spray coatings of powder materials*. Refer. Book. Kiev: Naukova Dumka.
2. Kharlamov, Yu.A., Budagiants, N.A. (2003) *Principles of the technology for repair and hardening of machine parts*. Vol. 1. Lugansk: V. Dal EUNU.
3. Borisova, A.L., Mil, I.V., Kajda, T.V. et al. (1995) Structure and properties of ferrochrome- and ferroaluminium-base coatings produced by electric arc metallising of flux-cored wires. *Avtomatich. Svarka*, **6**, 3–6.
4. Chevela, O.B., Morozov, I.A., Loginov, V.E. et al. (1975) Experimental study of plasma jet temperature. *Svarochn. Proizvodstvo*, **10**, 1–3.
5. Ageev, V.A., Buryakin, A.V., Buvajlo, V.V. (2003) Electric arc metallising unit KDM-4M. *Ibid.*, **4**, 43–48.
6. Voropaj, N.M., Kostenyuk, N.I., Markovich, S.I. (1998) Influence of easily ionised additives on characteristics of CO_2 AC pulsed-arc welding. *Avtomatich. Svarka*, **7**, 11–14.

INCREASE IN FATIGUE LIMIT OF WELD METAL IN APPLICATION OF REFINED COMPLEX ALLOY IN COATING OF ELECTRODES UONI-13/55

V.S. POPOV[1], I.M. BILONIK[1], S.P. BEREZHNY[1], M.V. SIDORENKO[1], A.A. SELEZNYOV[2] and V.V. POPOV[2]
[1]Zaporozhie National Technical University, Zaporozhie, Ukraine
[2]OJSC «Yuzhtsvetmetgazoochistka», Zaporozhie, Ukraine

It is shown that a complex ferroalloy used instead of traditional ferroalloys, i.e.deoxidizers, in electrode coatings leads to decrease in the content of non-metallic inclusions in low-carbon weld metal, increase in its short-time mechanical properties and fatigue limit.

Keywords: *electric filters, mechanism of vibration, vibrating beam, striker, anvil, cracks, ferroalloys*

In thermal electric stations, metallurgical plants and cement plants the settling electric filters are used for purification of air flow, dusted with suspended particles. Effectiveness and duration of their service depend greatly on the operation of a vibration mechanism realizing the removal of particles precipitated on the electrode. Working organs of the vibrating mechanism are a striker and anvil.

For welding of anvil to a beam of vibration the basic electrodes of UONI-13/55 type are used, providing the deposited metal with strength and ductile properties, maximum for non-alloyed steels. Nevertheless, cracks locating mainly in weld metal, were revealed in welds, joining the anvil with the beam of vibration (Figure 1). These cracks themselves do not cause the fractures of metal structures of an electric filter. However, as the beam of vibration plays a role of an elastic waveguide, their presence leads to the increase in dissipating properties of material and dispersion of impact impulse energy.

According to work [1], the coefficient of energy absorption is 5 times increased at a fatigue crack embracing up to 35 % of a console I-beam section. Consequently, the occurring cracks increase the damping properties of weld metal, as a result of which the drop of particles, trapped on receiving electrode, is not efficient enough that reduces the degree of purification of a dust-gas flow. The dust is sticked to electrodes, the increase in mass leads to a sagging of load-carrying structures and premature failure of the whole filter.

The aim of the present work is to study the causes of appearance of cracks in the spots of welding anvils to a beam of vibration and to develop the measures preventing their initiation and increasing the fatigue limit of the weld metal.

During the period of vibrating beam operation (5–7 years) it should withstand from $2 \cdot 10^5$ to $1 \cdot 10^6$ cycles of load, depending on vibration intensity [2]. Investigation of weld metal in spots of anvils joining with beam after the completion of service term showed that the initiation of microcracks is occurred in regions of clustering non-metallic inclusions (Figure 2). Under the conditions of elastic deformation of weld metal, the initiation and further propagation of cracks is provoked by transfer of an impact impulse of inclusion of an arbitrary shape of 1–20 μm. Avalanche and branched cracks are passed more often along the inclusions of type of tialite ($Al_2O_3 \times TiO_2$), helinite

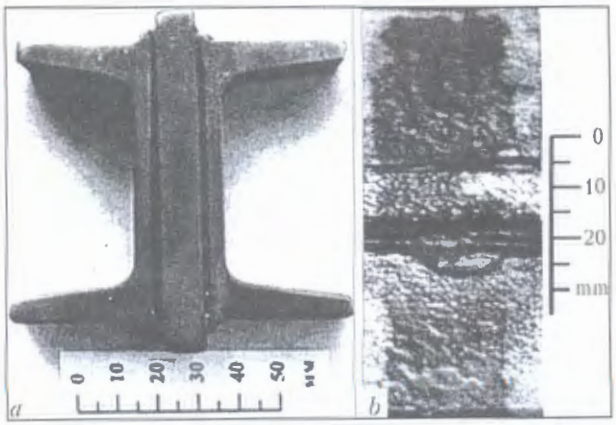

Figure 1. Cracks in weld metal made by electrodes UONI-13/55 in spots of anvils welding to vibrating beam observed in the process of repair: *a* — cross-section of beam; *b* — the same, top view

Figure 2. Series of cracks in the region of location of non-metallic inclusions in weld metal (×420)

($CaO \times Al_2O_3 \times SiO_2$) and perovskite ($CaO \times TiO_2$) (Figures 3 and 4).

Number of non-metallic inclusions in weld metal is much larger than in the parent metal and welding wire. Inclusions in weld metal are not only a product of deoxidation in the process of welding, but also a result of contamination of the charge materials, in particular ferroalloys in the composition of the electrode coatings. The coating of electrodes UONI-13/55 includes ferrosilicium FS-45, ferromanganese FMn-1.0 and ferrotitanium FTi30A.

It was shown in work [3] that in replacement of ferroalloys of industrial production in coating of electrodes UONI-13/55 by a complex refined ferroalloy of electroslag melting the content of impurities and non-metallic inclusions of tialite, helenite, perovskite and corundum types is reduced in the deposited metal. The decrease in content of non-metallic inclusions reaches 36 %, while that of refractory impurities, including aluminium oxide, reaches 50 %. Here, the formation of globular inclusion is occurred mainly [4], that influences to a lower extent the decrease in strength and ductile characteristics of the deposited metal. However, even the comparatively high characteristics of mechanical properties of weld metal, obtained at short-time static tests, are not a guarantee of the reliable performance of welds in structures subjected to impact and alternating loads during the required service period. At intensive impact load the fatigue fracture resistance is a decisive factor defining the strength and reliability of the welded joint.

The positive effect of metal refining in electroslag process on its ductile properties and fatigue limit is described in works [5–7]. To check the fatigue limit of metal deposited by electrodes UONI-13/55, whose coating contained a complex ferroalloy refined by electroslag method [3], the comparative fatigue tests of weld metal at symmetrical loading were made. Investigations were performed on butt welded specimens of steel St.3sp (killed), 23×150 mm size, 5 mm thickness with a 7 mm central hole. They were welded by industrial electrodes UONI-13/55 with a separate adding of ferroalloys into coating of electrodes and by experimental electrodes UONI-13/55, having a complex ferroalloy of electroslag melting in the coating. Specimens for welding were cut along the rolling direction. Plates were welded by a double-sided weld in a jig using 4 mm diameter electrodes at 160–180 A current and 24–26 V arc voltage. The reinforcement of non-heat-treated welded joints was machined flush with a parent metal.

Fatigue limits of specimens (Figure 5) was determined in a dynamic laboratory of Zaporozhie National Technical University in the unit of axial cyclic loading. Frequency of loading was 20–22 Hz, and accuracy of keeping the amplitude of loading – 3 %. Plotting of a left branch fatigue curve was made using the method of the least squares. Root-mean-square deviation of fatigue life for specimens welded by electrodes with a separate adding of ferroalloys and with a complex ferroalloy of electroslag melting, was 0.044 and 0.040, respectively.

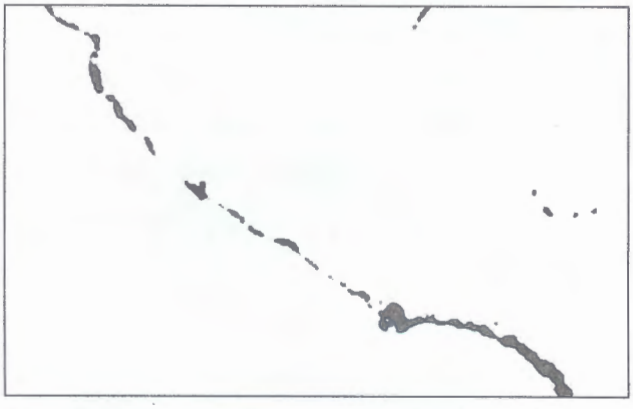

Figure 3. Crack passing through exogenous inclusions (×420)

Within the entire range of changing the loads the fatigue resistance of metal deposited with electrodes having a complex ferroalloy of electroslag melting is higher than that with electrodes having a separate adding of ferroalloys. With increase in number of loading cycles this difference in values of fatigue limit is, as a rule, increased to the benefit of welds made by electrodes with a complex ferroalloy in the coating.

The fatigue limits were determined using procedure given in [8]. The load pitch was 4 MPa. Fatigue limit of metal σ_{-1} deposited with industrial electrodes at a separate adding of ferroalloys was (86.9 ± 3.1) MPa, and root-mean-square deviation $S_{\sigma_{-1}}$ was 3.36. For metal specimens deposited by experimental electrodes with a complex ferroalloy of electroslag melting the fatigue limit reached (100.7 ± 3.4) MPa, and root-mean-square deviation was 3.25. The confidence intervals were obtained for probability of fracture equal to 95 %. Thus, the use of a complex ferroalloy of electroslag melting in the coating of electrodes UONI-13/55 guarantees the increase in fatigue limit of deposited metal by 16 %.

Stability of obtained properties was evaluated by the coefficient of variation of a mean value of fatigue limit $\overline{S}_{\sigma_{-1}} / \overline{\sigma}_{-1}$ characterizing the scattering of characteristics which occurred to be equal to 0.04 for weld metal made by electrodes with a separate adding of ferroalloys into the coating of electrodes and 0.033 for weld metal made by electrodes with a complex

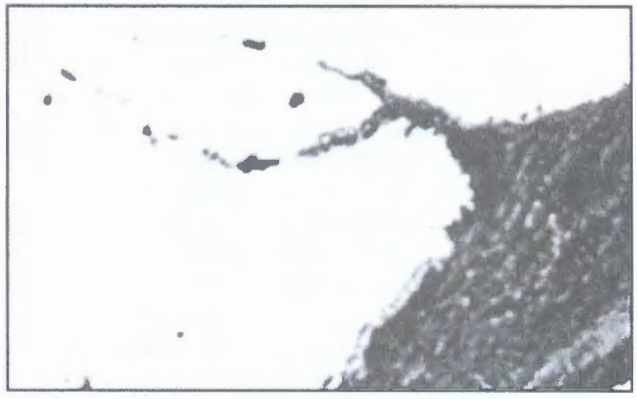

Figure 4. Branching of microcrack along non-metallic inclusions in weld metal (×420)

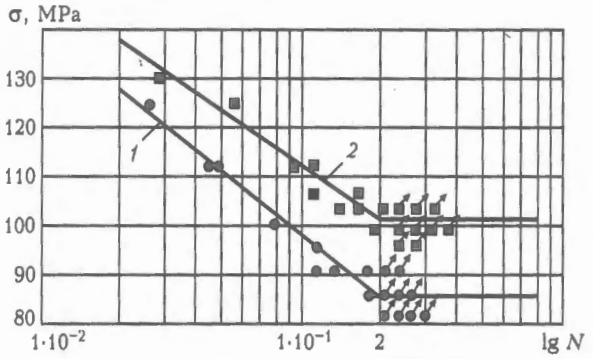

Figure 5. Results of fatigue tests of weld metal made by electrodes UONI-13/55: *1* – welded joint made by electrodes with separate adding of ferromanganese, ferrosilicium and ferrotitanium into coating; *2* – welded joint made by electrodes with adding of a complex ferroalloy of electroslag melting into coating

ferroalloy of electroslag melting. Thus, in use of a complex ferroalloy in the coating of electrodes UONI-13/55 the scattering of characteristics of fatigue limit of deposited metal is 1.2 times reduced.

The capability of metal of anvil–vibrating beam welds to withstand impact loads under the conditions of operation of vibrating devices of electric filters was evaluated from the results of testing full-scale components mounted on a special impact stand designed in collaboration with the Chair of Welding Equipment and Technology of Zaporozhie National Technical University and Open Joint Stock Company «Yuzhtsvetgazoochistka». Stand simulates the real energy parameters of impact load to which the vibrating beam of the electric filter is subjected.

Tests on base of $1 \cdot 10^6$ cycles of full-scale models in impact stand showed that in 18 % of welds made by electrodes UONI-13/55 with a separate adding of ferroalloys the crack were observed visually, which initiated in the root weld region and propagated in the deposited metal. In welds made by experimental electrodes with a complex ferroalloy in the coating the cracks were not observed visually after $1 \cdot 10^6$ cycles of tests.

Thus, in replacement of all ferroalloys in the coating of electrodes UONI-13/55 by a complex ferroalloy of electroslag melting the increase is observed not only in short-time mechanical properties determined in metal testing deposited by these electrodes, but also in fatigue limit of weld metal in the process of a long-time service at cyclic and impact loading as a result of decrease in content of non-metallic inclusions in weld metal.

1. Bovsunovsky, A.P. (2002) On the question of energy dissipation mechanism in fatigue crack. *Problemy Prochnosti*, **5**, 80–99.
2. Birger, M.I., Goncharov, A.E., Gordon, G.M. et al. (1982) *Electric precipitators in non-ferrous metallurgy*. Ed. by A.A. Gurvits. Moscow: Metallurgiya.
3. Popov, V.S., Bilonik, I.M., Berezhny, S.P. et al. (2000) Effect of composition of ferroalloys on the content and shape of non-metallic inclusions in metal deposited with electrodes UONI-13/55. *The Paton Welding J.*, **8**, 22–26.
4. Popov, V.S., Bilonik, I.M., Berezhny, S.P. (2000) Decrease in the content of harmful impurities in weld metal using the complex deoxidizing agent in coating of welding electrodes. *Materialoznavstvo ta Obrob. Metaliv*, **3**, 58–61.
5. (1981) *Electroslag metal*. Ed. by B.E. Paton, B.I. Medovar. Kiev: Naukova Dumka.
6. Ivanov, V.S., Gurevich, S.E., Kopiov, I.M. et al. (1968) *Fatigue and brittleness of metallic materials*. Moscow: Nauka.
7. Dogaeva, V.A., Georgiev, N.M., Anuchkin, M.N. (1966) Effect of refining by liquid synthetic slag on ductile properties of low-alloy structural steel. *Metallovedenie i Termich. Obrab. Metallov*, **11**, 17–20.
8. Stepnov, M.N. (1972) *Statistic treatment of mechanical test results*. Moscow: Mashinostroenie.

STRUCTURE AND MECHANICAL PROPERTIES OF WELDED JOINTS MADE UNDER THE WATER WITH FLUX-CORED WIRES

V.Ya. KONONENKO and A.O. KORSUN
«Ekotekhnologiya», Kiev, Ukraine

Effect of the content of nickel on mechanical properties of the joints produced by wet underwater welding using self-shielded flux-cored wires has been studied. It is found that nickel additives improve the mechanical properties of weld metal. Investigations of the composition of non-metallic inclusions proved the absence of adhesion between the inclusion and matrix in some of them. This is related to increase in the concentration of hydrogen accumulated at the non-metallic inclusion–matrix interface during the structure formation process. Presence of such «traps» may decrease the rate of hydrogen mass transfer in underwater welding. It has been found that a mixed ferrite structure of the weld metal characterized by chemical heterogeneity is formed at a nickel content above 1.2 wt.%.

Keywords: *wet welding, flux-cored wires, mechanical properties, non-metallic inclusions, weld metal structure*

It is known that during formation of welds made by consumable-electrode wet underwater welding, the metal is exposed to the following environmental impacts: intensive cooling (2 to 9 times higher than in welding in air [1–5]), high concentration of oxygen and hydrogen in the vapour-gas bubble [6, 7], higher pressure, transition of salts dissolved in the water into the metal at water evaporation in the reaction zone.

While intensive cooling promotes strengthening of the metal of welds made by wet underwater welding, high concentration of oxygen in the reaction zone leads to a practically complete burning out of the main alloying elements (carbon, silicon, manganese) [6–8]. Under such conditions increase of the mechanical and ductile properties of the metal of the joints can be achieved by correct selection of the alloying system.

Nickel is one of the elements successfully used for alloying of a number of steels [9]. Its addition increases the strength of interatomic bonds in the crystalline lattice of iron. It also promotes weakening of the carbon bond in the austenite lattice and enhances its diffusion coefficient [9]. Steel alloying with nickel decreases its brittle fracture susceptibility [10].

Known are examples of weld metal alloying with nickel, when developing self-shielded flux-cored wires for wet underwater welding [11–13]. Nickel was used in the alloying system of PPS-AN5 flux-cored wire [14]. However, a lowering of ductile properties of weld metal was found in welding steels 09G2 and 09G2S with this wire.

The purpose of this work is establishing nickel influence on the mechanical properties and structure of the metal of joints in low-alloyed steels, produced under the conditions of underwater welding with flux-cored wires with Mn–Al–Ce–Ni alloying system.

When the experiment was conducted, it was intended to perform welding with three flux-cored wires of rutile type (PPS-AN5 analog), to which 0.8, 1.2 and 1.6 wt.% Ni were added successively by decreasing the content of iron powder. Weight fraction of other slag-forming components was not changed. Flux-cored wires were made under the laboratory conditions. Their filling coefficient was 31–33 %, diameter being 1.6 mm. Butt joints were made with these wires in the downhand position at 0.6 m depth in fresh water in the recommended modes. ASUM-400 arc power source with a flat external volt-ampere characteristic was used. Total length of welding circuit of 70 mm^2 cross-section was 80 m. Base metal was 09G2 steel (0.093 % C; 1.48 % Mn; 0.27 % Si; 0.025 % S; 0.027 % P) 12 mm thick. Eight longitudinally arranged five-fold samples (their gauge diameter being 3 mm) for rupture testing of weld metal, as well as transverse macrosections were cut out of each of the produced butt joints.

Tensile testing of samples to fracture was performed in rigid tensile-testing machines UMM-5 and Instron-1250 (Instron Company, Great Britain), fitted with specially developed attachments, allowing thermostatting of the samples at the temperature from −196 up to +20 °C. During tensile testing the diagrams are recorded in force–time coordinates. Processing of loading diagrams and measurement of sample sections before and after fracture allowed determination of proof stress, $\sigma_{0.2}$, ultimate tensile strength σ_t, as well as relative reduction in area ψ. Analysis of the microstructure of weld metal and fractures was performed in JSM-840 raster electron microscope (REM) (JEOL, Japan) and JEM-200cx transmission electron microscope (TEM) (JEOL, Japan). Microanalysis was conducted in spectral and energy-dispersive spectrometers, incorporated in REM «Superprobe-733» (JEOL, Japan). Element distribution over the sample surface was analyzed using Digimap program. Hydrogen concentration was determined in XAS-2000 mass-spectrometer (Riber, France).

Table 1. Alloying element content (wt.%) in the weld metal determined with local probe analysis

Experiment No.	Nickel weight fraction in the charge, %	Fe	Mn	Ni	S
938	0.8	99.16	0.193	0.515	0.120
939	1.2	98.70	0.173	0.913	0.210
940	1.6	98.05	0.228	1.536	0.088

Note. Weight fraction of silicon in weld metal is 0.01–0.02 %, with traces of aluminium and cerium.

Results of local spectral analysis of weld metal are given in Table 1, and results of mechanical testing of samples — in Table 2.

The data in Table 1 indicate that the total amount of nickel added to the wire goes into the weld metal.

Analysis of the data given in Table 2 showed that increase of nickel content in the weld metal leads to improvement of the strength properties of weld metal with a certain deterioration of its ductile properties.

Metallographic analysis of the structure of weld metals with different content of nickel was performed. It was established that addition of nickel, alongside with refinement of the ferrite grain (Figure 1, *a*, *b* and *e*, *f*) also leads to increase of volume fraction of the acicular structural component (Figure 1, *e*, *f*). Increase of nickel content in the welds promotes formation of a certain structural inhomogeneity, namely regions of an acicular ferrite structure.

Analysis of the nature and distribution of non-metallic inclusions (NMI) in the weld metal showed that a large part of NMI is not connected to the ferrite matrix, but is separated from it by microcavities, which is readily seen in Figure 2. This is attributable

Table 2. Influence of temperature on mechanical properties of weld metals produced by flux-cored wire underwater welding with different content of nickel

T, °C	$\sigma_{0.2}$, MPa	σ_t, MPa	δ, %	ψ, %
Nickel weight fraction 0.8 %				
+20	373	451	14.2	46.2
–60	430	521	16.5	55.1
–120	572	603	11.1	60.3
–160	631	634	9.8	59.9
–170	634	642	7.4	40.2
–180	722	724	7.9	12.9
–196	713	713	0.2	0.7
Nickel weight fraction 1.2 %				
+20	375	458	12.5	31.1
–60	416	515	15.5	49.6
–120	560	606	13.9	61.6
–160	639	668	9.3	45.2
–170	651	656	2.3	11.6
–180	722	724	5.8	6.6
–196	713	723	0.2	0.7
Nickel weight fraction 1.6 %				
+20	378	464	7.2	27.2
–50	416	515	21.3	41.7
–120	475	557	15.4	51.5
–170	662	679	8.4	46.7
–180	682	693	4.3	24.3
–185	713	719	6.3	36.0

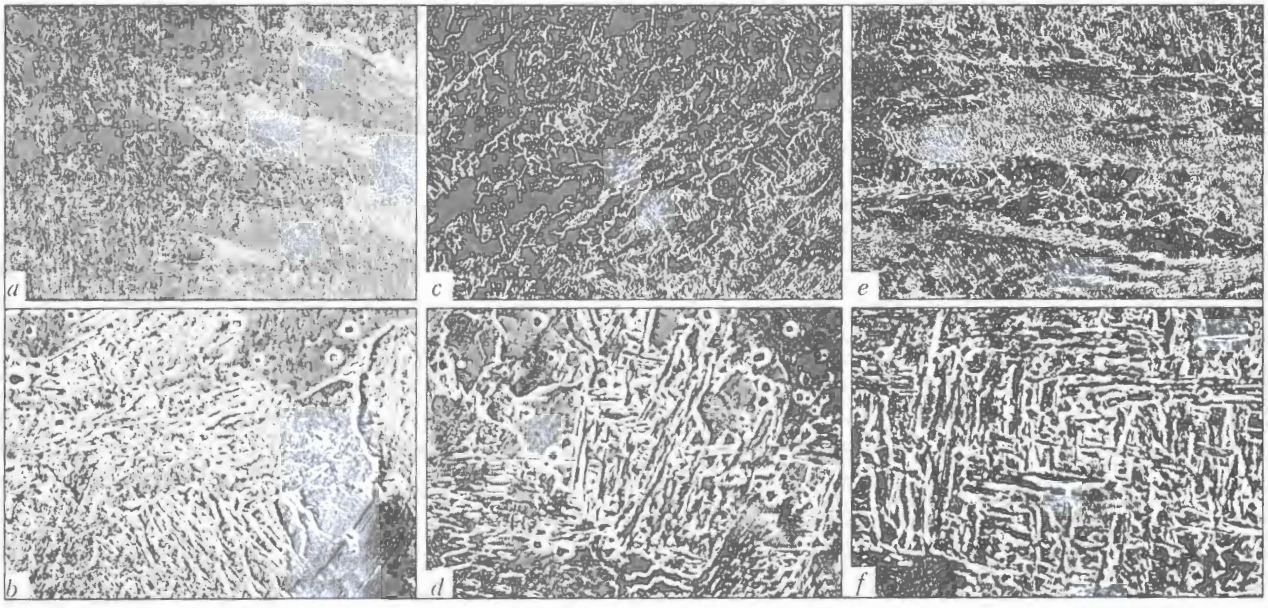

Figure 1. Microstructure of weld metal with different nickel content: *a*, *b* — 0.5; *b*, *d* — 1.0; *d*, *f* — 1.5 wt.% Ni (*a*, *c*, *e* — ×200; *b*, *d*, *f* — ×1000)

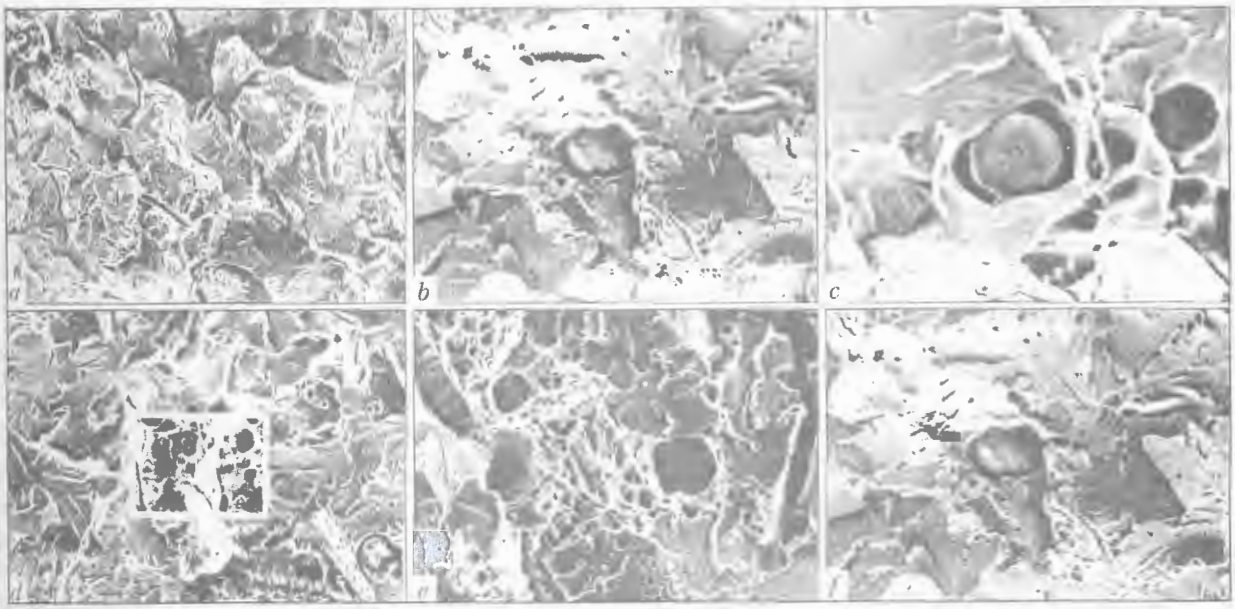

Figure 2. Fractograph of fracture surface of welds made under the water (*a* — ×500; *b* — ×1400; *c* — ×5000; *d* — ×900; *e* — ×1500; *f* — ×1700)

to the fact that the concentration content of elements is markedly reduced in the boundary region between NMI and the matrix (Figure 3).

This is confirmed by the results of investigations conducted in XAS-2000 mass-spectrometer. It is further established that a greater content of hydrogen was found in the structural regions with higher NMI content than that in the structural regions with a lower NMI content. Results of the conducted investigations lead to the conclusion that a significant amount of NMI is separated from the matrix by hydrogen-filled microcavities. Similar to welding in air with rutile type electrodes, such «traps» can change the hydrogen mass transfer rate in the weld metal [13]. Under the conditions of wet underwater welding mass transfer is slowed down with increase of the number of the «traps».

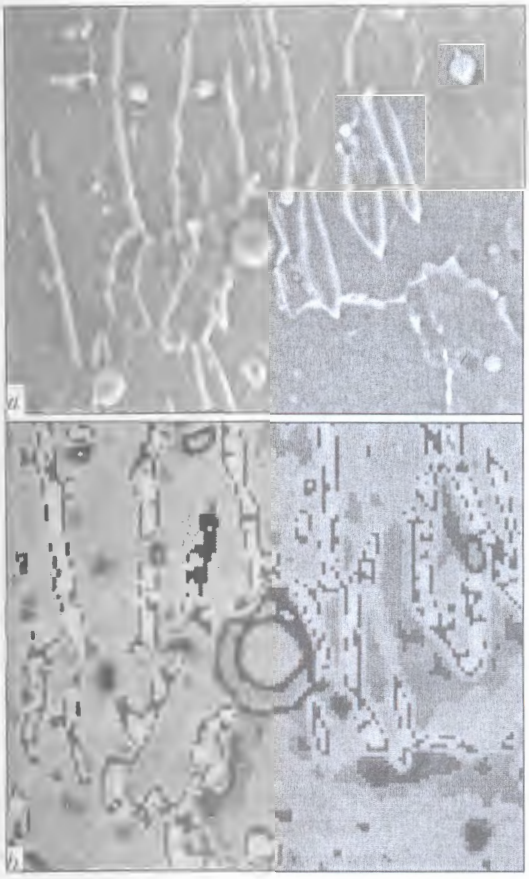

Figure 3. Nickel distribution in the weld metal produced by flux-cored wire with 1.5 wt.% Ni: *a* — studied structure; *b* — concentration map (×4500)

Investigations of NMI at large magnifications allow establishing the presence of structural regions along their edge, differing in phase composition (Figures 4 and 5). Most probably, these are regions of sulphur precipitation.

As follows from analysis results (Figures 6–8), the weld metal structure consists of a ferrite matrix and a phase with a higher content of carbon.

The characteristic distribution of the main alloying element, namely nickel, across the grain body also has a significant influence on the shape of the ferrite grain. Figures 3, 9 and 10 give the analysis zone and nature of nickel distribution between ferrite grains of different shape. As follows from the experimental results, given in these Figures, ferrite grains of an acicu-

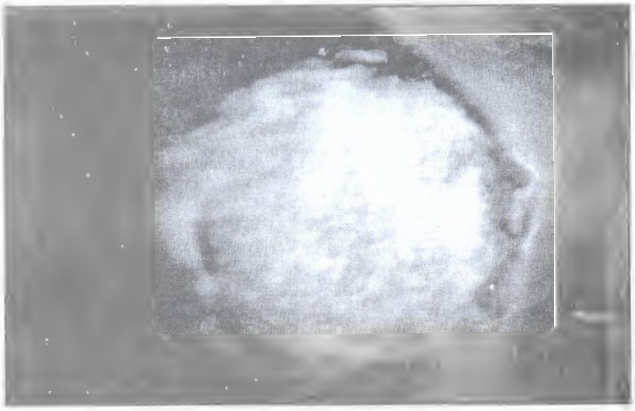

Figure 4. NMI in a ferrite grain matrix (×50000)

Figure 5. Light- (*a*) and dark-field (*b*, *c*) image of NMI in the metal of welds made under the water (×15000)

Figure 6. Diffraction patterns of the matrix (*a*), carbide phase (*b*) and grain structure (*c*) of the metal of welds made by underwater welding (×55000)

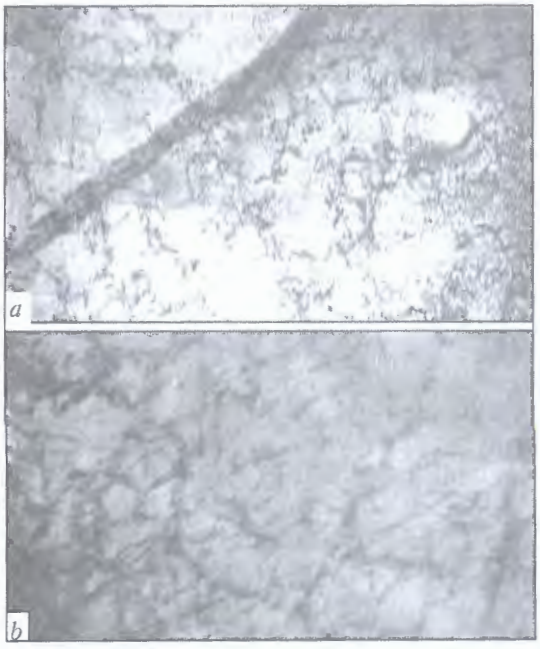

Figure 7. Grain microstructure in the metal of welds made by underwater welding (*a* — ×30000; *b* — ×8000)

Figure 8. Dark-field image of carbide phase in metal structure of welds made by underwater welding (×55000)

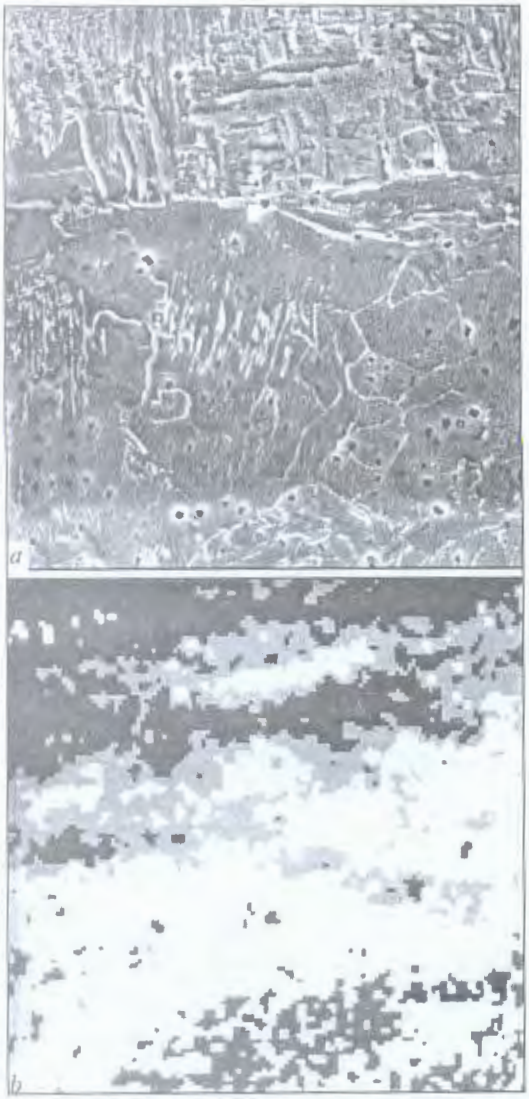

Figure 9. Nickel distribution between ferrite grains of different shape in the metal of welds made by underwater welding with 1.5 wt.% Ni wire (*a*, *b* — see Figure 3)

lar shape form at nickel content in the welds above 1.2 %.

It may be assumed that presence of a mixed structure in this case is related to chemical inhomogeneity of nickel distribution. An increase of nickel content is found in acicular ferrite grains, and, contrarily, a lowering of its content in the polygonal ferrite grains.

Therefore, in order to ensure higher mechanical properties of the joints produced by wet underwater welding, it is necessary to eliminate or minimize the concentration gradients of nickel in the weld metal structure. This can be achieved through a significant limitation of the content of the latter or increase of the weight fraction of manganese in the deposited metal.

CONCLUSIONS

1. Higher nickel content leads to higher strength properties of the metal of welds made by underwater welding, and somewhat lower ductile properties of the welds.

2. In some NMI there is no adhesion between the inclusion and matrix, which is, probably, caused by a higher concentration of hydrogen, which accumulates on NMI and matrix interface. Presence of such «traps» for hydrogen may lower its mass transfer rate during formation of welded joints in underwater welding.

3. At nickel content above 1.2 wt.% a mixed structure of weld metal forms with a chemical microinhomogeneity. Its level can be reduced by varying the proportion of alloying elements.

1. Savich, I.M., Melnik, Yu.P., Glukhova, E.V. (1978) Determination of temperature of electrode metal drops in underwater flux-cored welding. *Avtomatich. Svarka*, **9**, 12–14.
2. Savich, I.M., Kononenko, V.Ya., Gusachenko, A.I. (1984) Structure of weld metal and HAZ during welding in water of various salinity. *Ibid.*, **4**, 50–52.
3. Hasui, A., Suga, Y. (1980) On cooling of underwater welds. *Transact. of JWS*, **1**, 21–28.
4. Yara, H., Kikuta, Y., Matsuda, H. (1988) The TRC test for high-strength steel in wet underwater welding. *Ibid.*, **1**, 75–80.
5. Christensen, N. (1983) The metallurgy of underwater welding. In: *Proc. of Int. Conf. on Underwater Welding*, Trondheim, Norway, June 27–28, 1983.
6. Kononenko, V.Ya. (1993) Influence of electric arc process parameters in mechanized underwater welding on composition of vapor-gas bubble and oxygen and hydrogen content in weld metal. *Avtomatich. Svarka*, **11**, 18–21.
7. Kononenko, V.Ya. (1996) Metallurgical peculiarities of wet welding with flux-cored wires. *Ibid.*, **9**, 22–26.

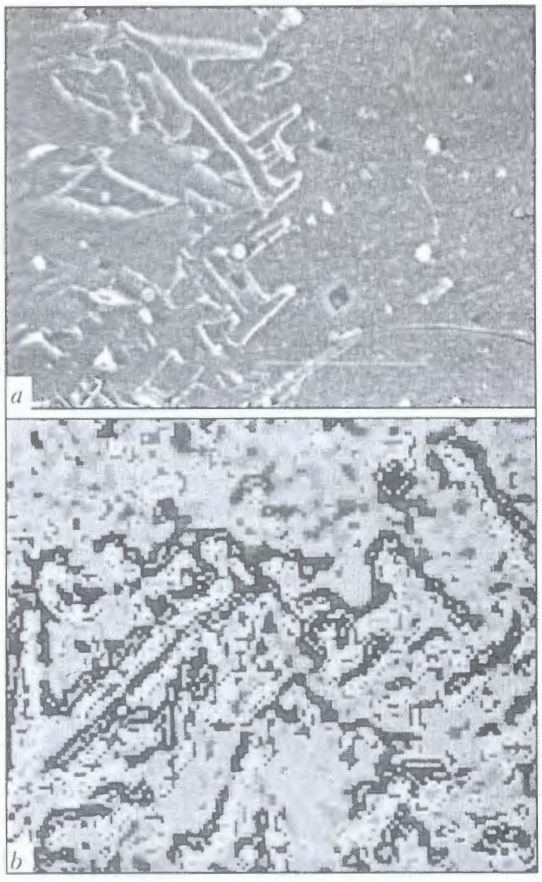

Figure 10. Nickel distribution between acicular and polygonal ferrite in the metal of welds produced in underwater welding with 1.5 wt.% Ni wire (*a*, *b* — see Figure 3)

8. Savich, I.M., Kareta, N.L., Grishanov, A.A. et al. (1982) Influence of cooling rate on distortions of metal lattice in welding under water and in air. *Ibid.*, **5**, 27–28.
9. Goldshtejn, Ya.E. (1968) *Low-alloy steels in mechanical engineering*. Moscow: Mashgiz.
10. Georgiev, M.N. (1973) *Toughness of low-alloy steels*. Moscow: Metallurgiya.
11. Asnis, A.E., Ignatushenko, A.A., Diachenko, Yu.V. (1983) Measures for hydrogen content reduction in heat-affected zone during mechanized underwater welding. *Avtomatich. Svarka*, **8**, 1–4.
12. Kononenko, V.Ya. (1987) *Technology of mechanized self-shielded flux-cored wire welding of low-alloy steel with σ_y up to 350 MPa in sea water*. Syn. of Thesis for Cand. of Techn. Sci. Degree. Kiev.
13. Gretsky, Yu.Ya., Maksimov, S.Yu. (1995) Influence of nickel on the structure and properties of welds in underwater flux-cored wire welding. *Avtomatich. Svarka*, **8**, 56–57.
14. Pokhodnya, I.K. (1998) Problems of welding of high-strength low-alloy steels. In: *Advanced materials science: The 21st century*. Ed. by I.K. Pokhodnya. Kyiv: Naukova Dumka.

APPLICATION OF ELECTROSLAG WELDING IN REPAIR OF BLAST FURNACE BODY AT OJSC «KGMK KRIVOROZHSTAL»

Yu.N. LANKIN[1], V.G. TYUKALOV[1], A.A. MOSKALENKO[1], A.M. GERASIMENKO[1], V.A. KOVTUNENKO[1], O.P. BONDARENKO[1], D.Yu. KUZMENKO[2], P.V. MARYSHEV[2] and G.N. CHABAN[2]

[1]E.O. Paton Electric Welding Institute, NASU, Kiev, Ukraine

[2]OJSC «KGMK Krivorozhstal», Krivoj Rog, Ukraine

Mechanical properties of metal of 45 mm thick 06G2B steel welded joint made by high-speed electroslag welding with additional concurrent cooling are presented. Selection of method of electroslag welding for enlargement of blocks and erection of a girth of a non-cooled part of a self-bearing housing in repair of the first stage of blast furnace DP-9 at OJSC «KGMK Krivorozhstal» was substantiated. The process flow diagram using the new machine AD-381 for site electroslag welding is described.

Keywords: *electroslag welding, housing of blast furnace, machine for site welding, sparsely-alloyed steel 06G2B of increased strength*

The largest in Europe blast furnace DP-9 of 5 000 m^3 capacity at OJSC «KGMK Krivorozhstal» was put into service in 1974. A self-bearing housing of the furnace was manufactured from steel of 16G2AF grade (ChMTU 1-349–68) of 40 and 45 mm thick class 440 of increased strength with a nitride strengthening.

In the process of continuous service under the severe specific conditions the deformations, defects and damages were accumulated in the furnace structures, requiring the replacement of some regions. To replace the areas of a non-cooled part of the housing, a plate rolled metal from the 06G2B quality sparsely-alloyed low-pearlitic steel of an increased strength (TS U 14-16-150–99), alloyed with microadditions of molybdenum, niobium, titanium, aluminium was selected. Steel of 45 mm thickness has yield strength of not lower than 440 MPa.

In accordance with the project of a capital repair of the first stage of the DP-9 blast furnace a unique technology was used for a self-bearing housing, consisting in replacement of the entire girth of 7 m height located at 30 m height and consisting of nine enlarged erecting blocks joined by vertical welds. Each erecting block was assembled of three panels. Welds between blocks and panels in blocks were performed by the electroslag method, which is characterized by high stability of the process proceeding. This promotes the producing of welded joints of a stable repeated quality. In addition, the absence of strict requirements to edge preparation, feasibility of use of standard welding consumables, high efficiency and economy make this method most adaptable for the fulfillment of long vertical butt joints of 30–60 mm thick metal, in particular in site conditions.

As steel 06G2B was used in construction for the first time, it was necessary to select such method of electroslag welding which could provide the required properties of welded joint under the site conditions. The successful experience of application of electroslag welding with additional concurrent cooling of 40 mm thick high-strength steels [1–4] gave an opportunity to recommend this method for producing welded joints of steel 06G2B of increased strength of 45 mm thick. To confirm this proper selection, the investigations of properties of welded joint metal were performed under the laboratory conditions at the E.O. Paton Electric Welding Institute. Wire Sv-10NMA (GOST 2246–70) of 3 mm diameter and welding flux AN-8 (GOST 9087–69) were used as welding consumables.

The aim of investigations was to determine the mechanical properties of weld metal and HAZ (yield strength, ultimate strength, elongation after rupture, impact strength, capability of welded joint to undergo a static bending, strength of the weakest region at static tension), as well as to study the macro- and microstructure of the welded joint metal.

Mechanical properties of metal of 06G2B steel welded joint, made by electroslag welding with a concurrent cooling (Tables 1 and 2), are not almost inferior to the same properties of the parent metal.

Macro- and microstructural analyses showed the absence of defects of structure, such as pores, cracks, lack of penetration, hazardous quenched structures and sufficiently uniform distribution of hardness in weld metal, HAZ and parent metal.

There were no cracks in specimens of welded joint metal subjected to static bend test (145° angle of bending).

Practical recommendations on technique and technology of high-speed electroslag welding with an auxiliary cooling of 45 mm thick 06G2B grade steel in repair of a self-bearing housing of blast furnace DP-9 at «KGMK Krivorozhstal» were worked out on the

Table 1. Results of tensile test of welded joint metal

Sampling place	*Yield strength, MPa*	*Ultimate rupture strength, MPa*	*Elongation, %*	*Reduction in area, %*
Weld metal	499.9–506.2 / 503.5	642.3–649.3 / 645.5	23.3–24.7 / 24.2	78.1–78.2 / 78.2
Parent metal	428.8–453.8 / 436.2	560.0–572.5 / 565.9	28.0–34.0 / 30.9	83.8–86.5 / 84.7
Welded joint	–	552.2–557.4 / 554.8	–	–

Note. Here and in Table 2 the numerator indicates the range of values, while the denominator indicates mean values.

basis of investigations. Main condition parameters are as follows:

number of electrodes, pcs 2
welding gap, mm ..... 24 + 2
welding current, A ..... 1200 ± 100
welding speed, m/h ..... 4 ± 0.5

The developed process flow diagram of repair works envisaged the arrangement on erection platform next to a furnace house of a specialized stand, designed and manufactured at «KGMK Krivorozhstal» for electroslag welding of enlarged erection blocks, equipped with replaceable racks and ladders for attending personnel. Three panels of 7000×2400 mm size were preliminary rolled by a required radius, and then assembled in the stand into an erecting block in a vertical position. An assembly gap was fixed by cramps, located from the concave side, and welding machine was moved along the guide rail (angle bar) mounted from the convex side of as-assembled erecting block. Run-in and run-out straps in electroslag welding were technological tolerances on panels, removed in cutting of the enlarged erecting block up to the required sizes. Tolerances were cut by a das-oxygen machine cutter with use of the welding machine carriage.

Check of assembly of all the enlarged blocks into an appropriate girth of the furnace housing was made on temporary stand located on the erection platform.

Table 2. Impact strength of welded joint metal (specimens with Mesnager notch)

Place of notch	*KCU, J/cm², at T, °C*	
	+20	*–40*
Weld	215.1–266.8 / 236.5	90.5–161.1 / 131.6
2.5 mm from fusion line	272.6–360.0 / 330.9	63.7–261.6 / 175.1
5 mm from fusion line	360.0 / 360.0	360.0 / 360.0
Parent metal	360.0 / 360.0	360.0 / 360.0

Position of separate blocks and the whole as-assembled girth both on stand and then on housing were checked using geodesic instruments. Then, a fragment was cut from the blast furnace housing girth, subjected to replacement. The accuracy of cutting was provided using a mechanized cutting by the machine oxygen cutter, mounted on the welding machine carriage.

Appropriate enlarged block was mounted on the place of the cut fragment and fastened by assembly devices and welding of upper and lower horizontal welds was made. Then, a next fragment was cut, another enlarged block was mounted, electroslag welding of vertical weld was made joining both

Figure 1. Electroslag welding of vertical joint of erecting blocks (view from erection suspension platform arranged inside the blast furnace housing)

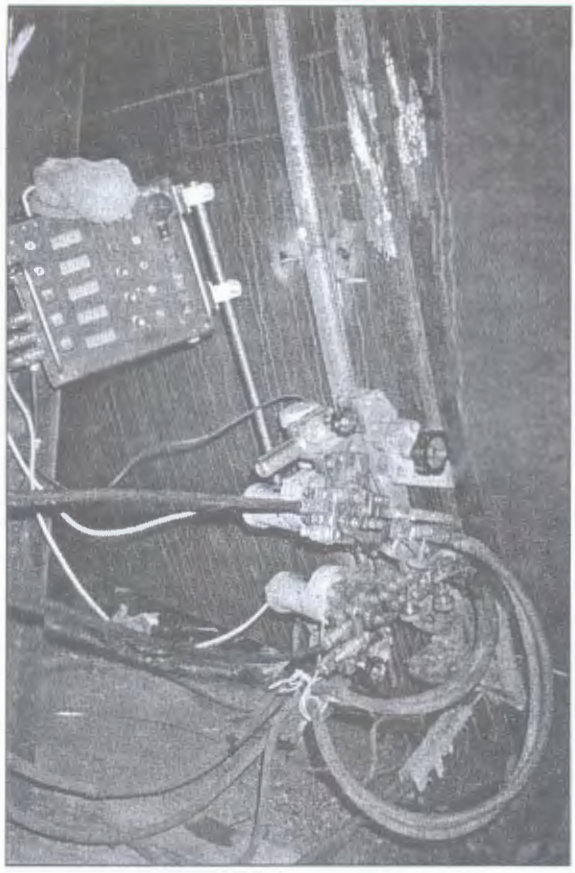

Figure 2. New two-electrode machine AD-381 for site electroslag welding of 30–60 mm thick metal

mounted blocks. Further, the welding of upper and lower welds joining the second enlarged block with housing was made. Then, one more girth fragment was cut, the next enlarged block was mounted, electroslag welding of weld, joining again the mounted block with previous one, and also the welding of joints between the block and housing were made. In such a sequence all nine enlarged blocks were erected and all nine vertical welds were welded by the electroslag method.

Each enlarged erecting block and housing element being dismantled were transported by an erecting crane through a cupola part of the furnace. The process flow diagram envisaged the movement of the welding machine along the inner surface of the body. Moreover, the guiding rack (angle bar) of the machine was mounted on as-welded-in erection block. This made it possible (in case of need to make a required assembly gap) to use the machine carriage as a base for gas-oxygen cutter. The assembly gap for the electroslag welding between the erecting blocks was fixed by assembly cramps mounted from the external side of the body. Welding machine, power sources, cassettes with welding wire were arranged on a suspended platform beside the weld inside the blast furnace body (Figure 1).

To realize the developed process flow diagram with allowance for peculiarities of welding condition parameters (welding speed was increased up to 4 m/h), the new machine for the site electroslag welding AD-381 was designed (Figure 2) [5]. Quality of all the welds was inspected by visual-optical and ultrasonic methods of control. Places of completion and intersection of welds were additionally controlled by gammagraphy. Before putting the furnace into operation, the tests of a self-bearing housing for strength and air-tightness were performed in accordance with requirements of SNiP III-18–75.

Thus, owing to the strict keeping the technology developed the unique operation of replacement of damaged metal of blast furnace housing girth by the new high-strength sparsely-alloyed steel of 06G2B grade was realized in the scheduled terms.

All vertical enlarging and site joints were made by a high-speed electroslag welding with additional concurrent cooling. Total length of all these welds was 140 m, i.e. ≈ 60 % of mass of metal deposited by different methods of welding in repair of the housing.

Specialized machine of the new generation for the site electroslag welding of 30–60 mm thick metal was tested successfully under the industrial conditions.

The application of electroslag welding in parallel with high process efficiency made it possible to produce the required properties of the joints.

1. Musiyachenko, V.F., Kasatkin, B.S., Mikhodui, L.I. et al. (1982) Welding of high-strength steel 12GN2MFAYu. *Avtomatich. Svarka*, **5**, 47–50.
2. Sushchuk-Slyusarenko, I.I., Khrundzhe, V.M., Lychko, I.I. et al. (1978) Selection of cooling conditions in electroslag welding of steel 14Kh2GMR. *Ibid.*, **7**, 43–45.
3. Sushchuk-Slyusarenko, I.I., Moskalenko, A.A., Khrundzhe, V.M. et al. (1983) Electroslag welding of steel 12GN2MFAYu of 40 mm thickness. *Ibid.*, **11**, 58–59.
4. Khakimov, A.N. (1984) *Electroslag welding with control of thermal cycles*. Moscow: Mashinostroenie.
5. Kovalyov, V.D. (2003) Automatic machine AD-381 for electroslag welding with forced formation of vertical joints. *Svarshchik*, **4**, 3.

FATIGUE DAMAGES OF WELDED CRANE BRIDGES

O.A. EMELIANOV[1], V.P. SHEPOTKO[1], Yu.V. PIKHOTA[1], S.V. LUBENETS[1] and A.G. BURENKO[2]
[1]Donbass State Engineering Academy, Kramatorsk, Ukraine
[2]Company «Novokramatorsk Machine-Building Plant», Novokramatorsk, Ukraine

Results of analysis of fatigue damages in welded bridges at 1500 cranes covering a period of the last 25 years are presented. The need to revise approaches to methods and principles of design, fabrication and calculation of welded bridge structures is noted.

Keywords: *welded structures, welded bridges of cranes, concentration of stresses, alternating stresses, vibration, cyclic fatigue life*

Since the beginning of use of welding technologies in crane construction, they were constantly improved to increase the strength and cyclic fatigue life of welded joints.

However, as the results of diagnostics showed, these works, made during 50 years, did not always contribute to a significant increase in life of welded crane bridges.

Welded joints on crane bridges during service have much lower and rather instable fatigue resistance, than that determined in lab conditions in testing full-scale specimens for the same load conditions.

Fatigue cracks are revealed usually on all the areas of welded bridges, in particular in those places where there are different design elements welded to beams or technological cuts made in elements for providing welds (Figures 1–4).

In riveted crane bridges the cracks can initiate after the long-term service. For example, at Company «Novokramatorsk Machine-Building Plant» 150 cranes of «Skoda» company with riveted bridges of 1933–1935 years of manufacture, are operating until now, in which the running wheels, bearing units, gearing in reduction gears of drives and different units in electric equipment were replaced, however, there were no damages in metal structures of bridges.

Crane constructors state on the basis of the experience of service of riveted and welded bridges that the causes of observed reduction in cyclic fatigue life of welded bridges can be only the thermophysical and chemical-metallurgical actions on weldments, resulting in the formation of local differences in chemical composition, structure and geometry, leading to deterioration of mechanical properties and increase in concentrations of stresses, and also residual stresses and plastic deformations in a near-weld zone. Therefore, the problem of increase in fatigue life of structures should be solved by specialists-welders.

Fatigue damages of welded crane bridges, except corrosion ones, reach 100 % of their premature failures and are a main factor defining the fatigue life of these structures [1, 2].

Laboratory of technical diagnostics of Donbass State Engineering Academy (DSEA) carries out in-

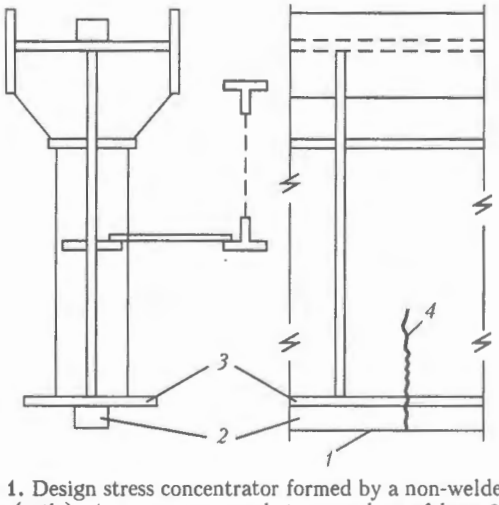

Figure 1. Design stress concentrator formed by a non-welded butt of bars (rails): *1* – narrow gap between edges of bars *2; 3* – beam chord; *4* – crack in chord

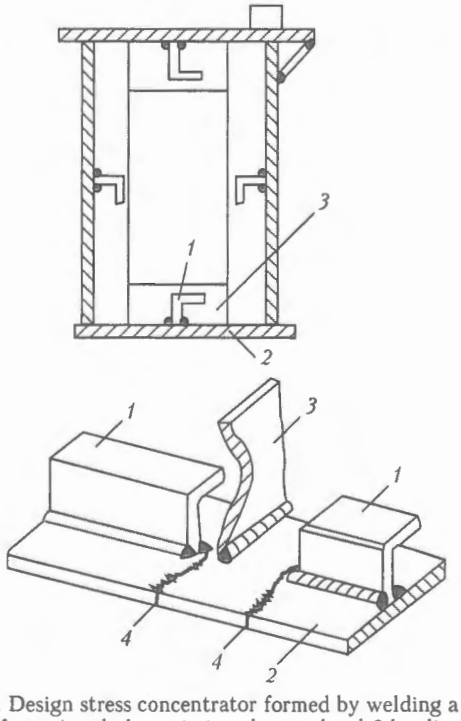

Figure 2. Design stress concentrator formed by welding a longitudinal stiffener *1* and elements to a lower chord *2* by diaphragm *3* with a relatively small gap between them; *4* – cracks

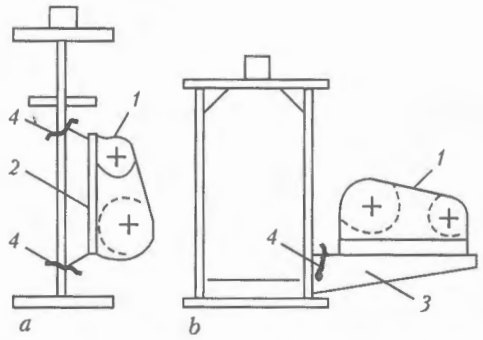

Figure 3. Design stress concentrator formed by fastening of frame (*a*) or bracket (*b*) to plate of main beam wall: *1* — reduction gear; *2* — frame; *3* — bracket; *4* — cracks

vestigations since 1978 on the creation of rational welded structures of load-carrying constructions. During past 25 years 1500 overhead travelling cranes were diagnosed. It was established that up to 60 % of inspected machines have fatigue damages, forming, as a rule, in places where calculations, made using the generally-accepted procedures, and strain measurements under service conditions show a low level of stresses from loads, caused by lifting-lowering of weights and their transporting along the main beams, i.e. in those places where their appearance was not predicted.

Moreover, the damages of extended most loaded lower chord of main beams were revealed only in six cases and caused by a non-rational design of welded sub-assemblies and lamination of plate of chords (see Figures 1–3).

The causes of damages of bridges, according to the results of analysis, were due to the presence of concentration of stresses in some welded joints, defects in welds and reduction in steel ductility, caused by a strain ageing [1].

The investigations showed that most welded sub-assemblies in crane bridges, where the fatigue cracks were formed, were subjected to action of cyclic loads from lifting-lowering of weight and displacement of carriage with a weight, however, these loadings until the moment of crack formation were few and could not lead to fracture.

Similar situation is observed in service of spans of railway bridges [3]. To clarify the causes of fatigue damages of welded crane bridges, it is necessary to take into account objectively the competence of assumption, according to which a cyclic fatigue life of crane bridges can be defined only by loads occurring in the process of lifting-lowering of weight and its transportation by a carriage along the main beams of bridges, i.e. by loads only from change in level and place of applying forces of mass of load and carriage.

During crane designing it is necessary to take into account the following two criteria:

- the value of design deflection of main beams in the middle of span (rigidity of beams) at the action of dead weight and mass of loaded carriage;
- allowable level of stresses in beam.

Numerous calculations for strength confirm that stresses from alternating load on main beams of general-purpose cranes of load capacity from 5 up to 50 t and of a span from 10.5 up to 34.5 m have asymmetrical cycle with a coefficient of asymmetry $r = \sigma_{min}/\sigma_{max} = 0.2–0.4$. Assurance of design rigidity of main beams of bridge $[f] = L/k$, where f is the allowable deflection of beam; L is the crane span; $k = 600–700$ is the coefficient, depending on the operation condition of crane operation will cause the decrease in values of design stresses in a lower tension chord of beam to values $\sigma = 110–120$ MPa. Fatigue limit $R_{0.25}$ at loading by asymmetrical cycle with a coefficient of asymmetry $r = 0.25$ on the base of tests $N = 2 \cdot 10^6$ cycles is equal to 126 MPa [4] at the condition that the welded joint is butt, intersecting with a longitudinal weld. This joint is similar to butt joint of the chord, intersected by a weld that fastens the wall sheet to the chord, i.e. $\sigma_{max} < R_{0.25}$, where $R_{0.25} = 126$ MPa is the design fatigue resistance of low-carbon steel.

If to assume that crane is operating continuously all the year and each its cycle is equal to 10 min, then it will fulfill during a year $T = 360 \cdot 24 \cdot 60/10 = 51840$ cycles and it should operate $A = N/L = 2 \cdot 10^6/51840 = 39$ years before the appearance of the first crack.

In practice, the high cyclic fatigue life of the most loaded middle cross-section of main beams of travelling cranes in lifting-lowering and transportation of

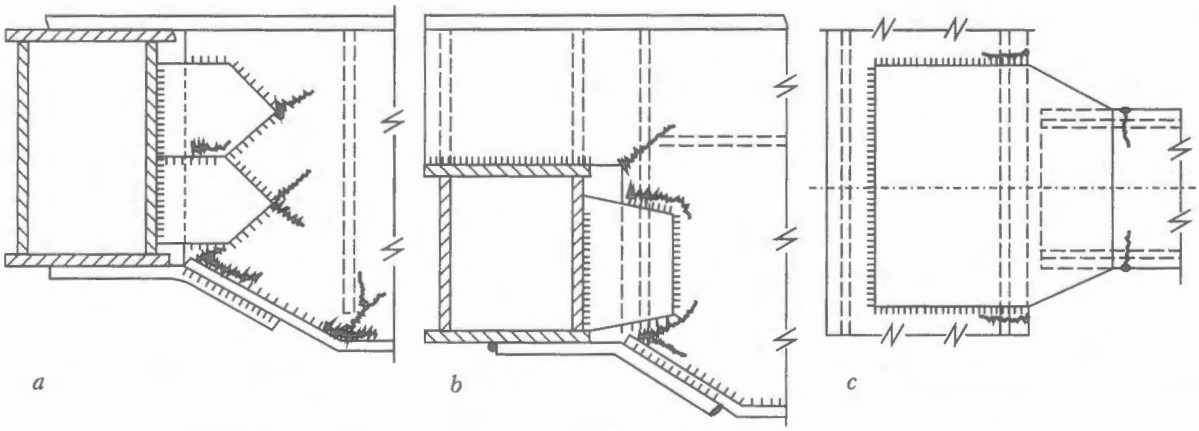

Figure 4. Design stress concentrators of different types (*a–c*) formed by welding-on of different elements and technological cuts (wavy lines show cracks)

weights by the carriage, i.e. at the action of principal stresses, is confirmed.

Then, the question is arisen how to explain the numerous fatigue damages of other low-loaded places of structure.

The opinion is expressed in article [3] that the fatigue cracks can appear in welded different-purpose structures, corresponding to the requirements of present effective standards of designing and manufacture, even at the early stage of the operation. Consequently, there are additional negative factors reducing the fatigue resistance of welded structures which are not taken into account by the existing methods and standards of designing.

These factors include, first of all, the loads causing the secondary stresses [1, 3], vibration of structures and their separate elements. Over the recent years, the new proofs of importance of allowances for vibrations in designing of welded structures of crane bridges were obtained. Therefore, the radically new revision of approaches to the procedure and principles of designing, manufacture and calculations of welded structures of crane bridges as regards to their fatigue resistance is required.

The importance of the soonest solution of these problems is confirmed by the results of investigations obtained by DSEA and other research organizations. Some new statements, established in DSEA [1], are given below:

- place of initiation and configuration of main part of fatigue cracks prove that they are formed by the action of loads caused mainly by a force interaction of crane wheels with rails in its movement along the tracks;
- damage of welded bridges occurs, as a rule, at intensive wear of wheel flanges caused by the action of transverse forces in wheel–rail contact in movement of cranes having an erecting misalignment of running wheels in a horizontal plane, i.e. when the force interaction in wheel–rail contacts initiates the high-frequency loads [1, 5];
- transverse loads are the sum of two (or several) alternating forces acting on the crane wheels both in horizontal and also in vertical planes, and produced by superposition on an alternating component (Figure 5) with a low frequency and high amplitude of high-frequency components with lower amplitudes [6, 7];
- low-frequency component is energized during the crane movement along the rails mounted with deviations in height. Levels of amplitudes of low-frequency components are directly proportional to torsional rigidity of the bridge and difference of deviations of rails in height in one transverse section of the span. High-frequency components, acting in horizontal plane, are energized in rolling of wheels having an erecting misalignment in horizontal plane [6], while in vertical plane they are energized in crawling out the wheel flanges upward and subsequent drop downward along the lateral face of rails [1];

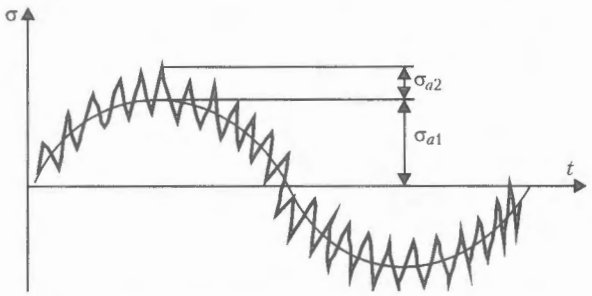

Figure 5. Scheme of cycle shape at two-frequency load (σ_{a1}, σ_{a2} – amplitudes, respectively, of low- and high-frequency components of loads)

- the cause of vibration appearance can be unproper alignment and balancing of rotating parts of drives, and also the contact of wheel pair gears in reduction gears;
- the cyclic fatigue life of the welded bridge in action of two-frequency (or polyfrequency) load, produced by superposition on alternating component with a low frequency and high amplitude of high-frequency components with lower amplitudes, can be significantly reduced, if the place of vibration source (wheel–rail, reduction gear contacts), located closely to weld, is subjected to the action of a low-frequency component (slipping parts of end beam, place of abutting main beams to end beams, site welds of end beams). The formation of two-frequency loads on travelling cranes is described more in detail in work [1].

There is an opinion that the formation of cracks in above-described cases can be caused by secondary stresses which are taken into account in generally-accepted procedures of strength design in structures [8]. These stresses are formed often as a result of combined deformations of elements incorporated into welded sub-assembly or structure and having different rigidity. As follows from article [3], the secondary stresses proper cannot lead to the decrease in the fatigue life, but this decrease is quite explainable if to take into attention that the higher high-frequency stresses from vibration of elements are superimposed on the secondary low-frequency stresses (Figure 6). This total action of two-frequency (or polyfrequency) loads is to be taken, as a whole, as «single type of external action».

The study of causes of fatigue damages of nuclear reactors and submarine hulls showed also that two- and polyfrequency (in general case) loads [8] decrease significantly the cyclic fatigue life of materials and joints.

Methods of improvement of fatigue resistance of welded joints and structures can be divided into three distinguished groups, such as improvement of fatigue resistance by a local treatment of welds, rational design of welded sub-assemblies and rational schematic-design solution of crane bridges as a whole.

First group of methods. It is described comprehensively in works [3, 6] and widely used at present for improvement of fatigue resistance of welded joints. It is based on decrease in concentration of stresses in

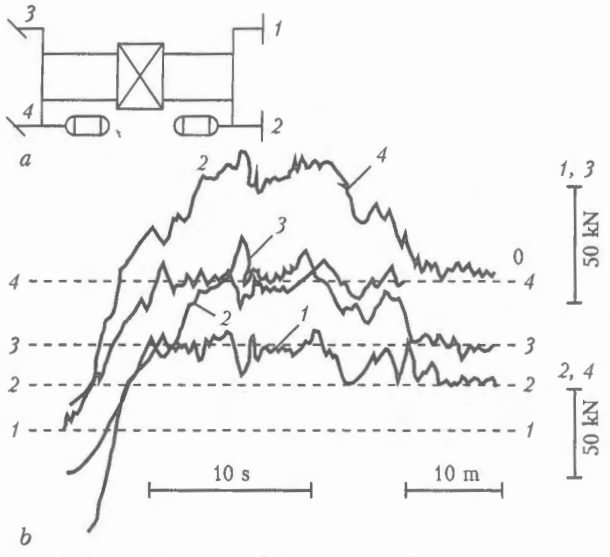

Figure 6. Shape of cycle of polyfrequency loading of running wheels of travelling crane: *a* — scheme of misalignment of wheels; *b* — oscillogram of wheels loading; *1–4* — numbers of wheels

places of weld metal transition to the parent metal, where the fatigue cracks are more often formed, or on artificial inducing of residual compressive stresses in surface layers of weld and HAZ.

The second group of methods. It is described comprehensively in works [1, 9, 10]. The methods are based on rational design of welded sub-assemblies incorporated into the crane bridge. This makes it possible to provide the uniform transfer of force in design elements of the bridge, included into sub-assembly, i.e. to eliminate the concentration of stresses by a proper design within the limits of the welded sub-assembly and elements, adjacent to it, to reduce the effect of residual stresses on fatigue resistance of welds and sub-assembly, as a whole, to prevent the strain ageing of steel in welded joints. Their rational and sufficient application in designing machines depend of qualification of the designer, i.e. an engineer-specialist on hoisting-transportation machinery who should have an appropriate education and training.

The third group includes the methods of prevention of factors [1, 9] causing the fatigue damages of welded bridge in its movement along the span, which are based on the improvement of schematic-arrangement solution of the bridge and crane, as a whole, to eliminate and decrease significantly the range of reactive forces in wheel–rail contacts, i.e. to prevent the change in forces and stresses in bridge design in movement of the crane along tracks having deviations from design sizes and also the feasibility of the vibration appearance.

The investigations, made in DSEA, showed that the main factor allowing prevention of the appearance of alternating forces (and stresses) in the process of the crane movement is the travelling quality of the cranes.

During the crane movement along the tracks the mass loads on the bridge are not changed in level and place of applying. The alternation of loading is occurred due to the range of vertical reactive forces, caused mainly by the crane movement along tracks having unevenness in height, and change in horizontal reactive forces in rolling of wheels mounted with a misalignment [1, 9]. Consequently, the bridge loading can be reduced by equalizing the vertical and decrease in horizontal reactive forces. All the methods, allowing solution of this problem, can be named as «improvement of travelling properties of cranes».

Travelling properties of the crane (load carriage) mean its capability to fulfil the hoisting-transportation operations by moving along the tracks without contact of flanges with lateral faces of rails and slipping of driving wheels, to have equal vertical loads on wheels within the limits of each end beam of the bridge, minimum lateral forces in wheel–rail contacts and minimum loads from units of drive for crane travelling on metal structure of the bridge.

The travelling properties of the crane are defined by adaptability of its design in moving the crane trestle, by capability to preserve a stable straightlinear movement without contact of flanges, not to create (and not to receive) the lateral horizontal forces on wheels, bridge and crane track in the process of operation and movement.

The crane adaptability to track means its capability to move freely along the rails of trestle, mounted with deviations from rated design sizes in horizontal and vertical planes, without contact of flanges with rails and redistribution of vertical loads on wheels.

Analysis of damages of welded crane bridges showed the following cause, not depending on welding, but influencing the travelling properties and loading in the crane movement:

- rationality of schematic-arrangement solution of the bridge, as a whole, design of welded sub-assemblies of the bridge, design of drives of the crane movement;
- rigidity of bridge plane displacement (plane displacement is the off-plane deformation of the framework);
- accuracy of mounting of crane tracks, assembly of crane bridge and mounting of running wheels of crane (carriage) in horizontal plane;
- friction forces in running wheel–rail contacts, i.e. non-holonomicity and non-stationarity of couplings in kinematic pairs of wheel–rail due to effect of elastic slipping on their force interaction;
- secondary stresses;
- elasticity forces of separate sub-assemblies and bridge as a whole, influencing the energizing of vibration in the crane, its frequency and amplitude;
- quality of setting electrical circuits of drives.

The above-mentioned factors contribute in movement of cranes to the appearance of a low-frequency component with a high amplitude and vibration loads and, finally, to the fatigue damages in low-loaded places. Their elimination increases significantly the cyclic fatigue life of the bridge that proves the comparatively low effect of welding consequences on the fatigue resistance. In this situation the fatigue

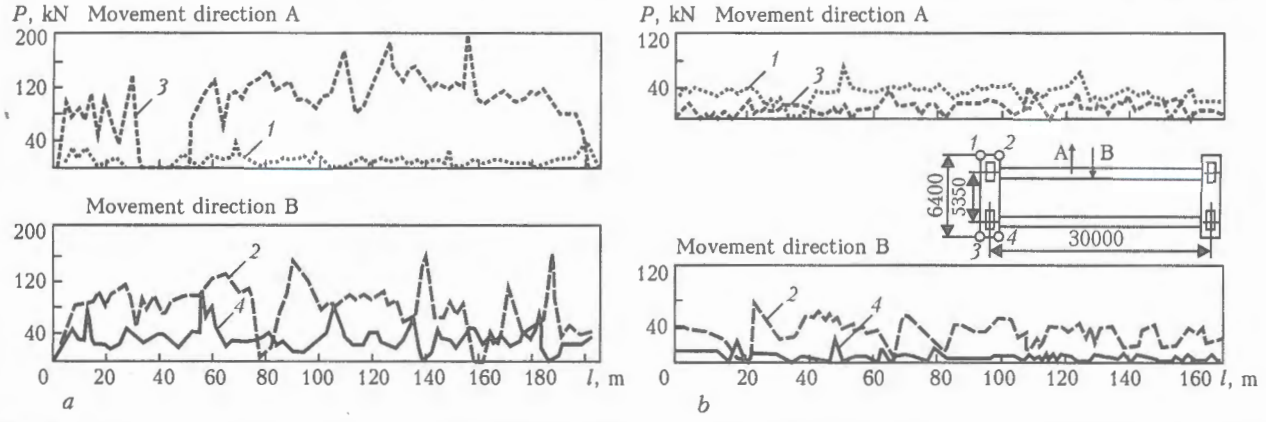

Figure 7. Lateral loads P on retaining rollers of travelling crane: *a* — wheels with misalignment; *b* — misalignment of wheels is eliminated; *1–4* — numbers of rollers; l — length of beam

strength is defined only by the design drawbacks, the successful elimination of which, is the prerogative and wide field for the activity of specialists on hoisting-transporting machinery.

Three methods of improving the fatigue strength of welded structures were above-mentioned. The first one, the treatment of welds, increases the fatigue resistance of metal of weld proper and HAZ. The second one, the method of design, increases the fatigue life of the welded sub-assembly by the more favourable transfer of force into its cross-sections.

Both these methods are passive, as they do not effect on total loading of crane trestle, and also on non-efficient losses of energy consumed for the crane travelling.

The third method, also design one, reduces the loading of bridge and crane trestle in crane movement (Figure 7), and also non-efficient losses of energy, reduces or eliminates the range of amplitudes of forces and stresses in structure. Method is based on improving the travelling properties of the crane.

Let us consider the loading of crane bridge in the process of operation.

It was shown that assurance of standard rigidity of main beams of bridge $[f] = L/k$, $k = 600–700$ by increasing the moment of resistance against bending will cause the decrease in level of normal stresses in beam up to values $\sigma_{max} < R_r = 126–161$ MPa.

Thus, the highest stresses will not exceed the fatigue limit, determined on the base of $N = 2 \cdot 10^6$ cycles, here, only the low-frequency load with the highest

Design shapes of main beams

Framed (truss)	*Plate box-type*	*Plate I-beams*
Main *1* and auxiliary *2* frameworks, joined by horizontal upper *3* and lower *4* frameworks	With two solid walls with a brake block *1* or without it	I-beam *1* and auxiliary framework *2* joined with horizontal frameworks *3* and *4*
Two main frameworks *1* and *2* joined by horizontal upper *3* and lower *4* frameworks	With one light-weight wall with cuts *1*	I-beam *1* with developed upper chord and fenced framework *2*

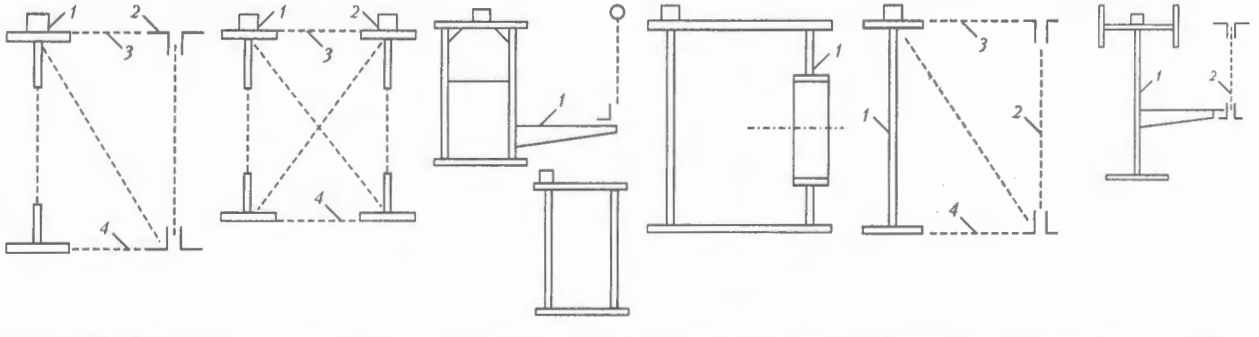

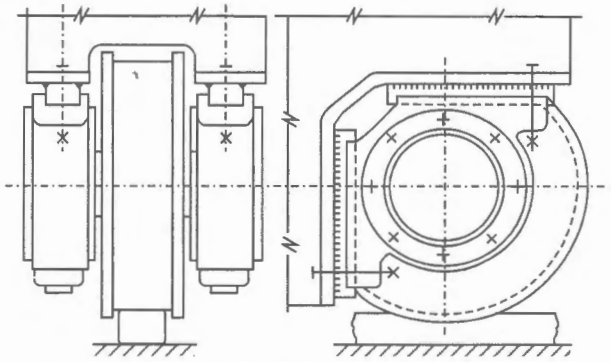

Figure 8. End beam with rolled-out wheels

amplitude σ_{max} is acting on bridge. The experience of service shows that the operation of mechanisms of hoisting and movement of the carriage does not energize vibration and does not lead to the appearance of two-frequency load. Consequently, there are no reasons for accelerating the appearance of fatigue damages caused by main loads, bending the main beams.

The fatigue cracks can be formed only under the action of secondary stresses, i.e. by pressing through the plate of the upper chord by rail, breakaway of lugs connecting rail to beam, breakaway of blunt rests of the carriage, cracks in places of welding frame brackets to the beam walls for mounting drives and cabinets with electric equipment, in places of fastening main beams to end beams and so on.

Causes of damages of main beams are described comprehensively in manuscripts [1, 9]. In some cases the cracks in elements of main beams (from action of secondary stresses) begin to propagate rapidly under the action of main stresses from main beam bending.

It is evident that it is possible in these cases to prevent the fatigue damages of main beams, caused by loads in handling of weight by a hoisting winch and carriage, by eliminating factors which cause the occurrence of the secondary stresses.

In crane movement along the span at a constant level and place of applying forces of load mass and carriage the low-frequency components can be formed only by changing the support reaction of the crane in its movement along the tracks having differences in height.

Range of values on vertical support reactions can be within $0 \le P_v \le \alpha 2P_v$ (P_v — the highest vertical load on wheel at carriage position in the span middle; α — coefficient allowing for increase in this load in case of carriage approaching the end beam, difference of values P_v in the limit of one end beam) and depends on torsional rigidity of the bridge frame. Table shows the cross-sections of basic types of main beams which greatly differ by a torsional rigidity.

Bridges with a low rigidity of plane displacement or with articulated joints («pliable») have more stable value of support reactions, which are not subjected to effect of deformability of structure in the process of movement, therefore, there are no reasons for the formation of low-frequency load and, consequently, the two-frequency loads.

Three methods were above-mentioned, providing the elimination of fatigue damages of welded crane bridges, from which the third one is most profitable, from the economic point of view, and promising. Its main advantage consists in the fact that it makes possible to eliminate the alternation of bridge load from changing the level of vertical reaction in crane movement along the tracks having differences in height, or sliding out the wheel flanges on lateral faces of rails and changing the horizontal support reactions in rolling of wheels mounted with a misalignment [6].

Action of two-frequency load is rather undesirable for the structure, as it reduces greatly the fatigue limit. It is possible to attain the required fatigue life by eliminating the low-frequency component either of vibration or both by improving the travelling properties of the crane.

After 1945, when the mass manufacture of crane bridges started in a welded version, their frequent damages showed that a simple copying of the shape of riveted sub-assemblies and structures for mating the components in them using welding is inadmissible.

Framed structures of bridges, used widely earlier, began to be replaced by solid-walled structures with a closed cross-section of box-type beams, that was stipulated by a wide implementation of the automatic submerged arc welding. In the middle of the 1950s a standard design of slipping blocks of running wheels was widely used to apply the roller bearings, which deteriorated greatly the accuracy of mounting wheels and strength of load-carrying structures in places of slipping blocks fastening (Figure 8). Weakening of support blocks and increase in misalignment of wheels in horizontal plane contributed to different mass damages of bridge structures, intensive wear of flanges of running wheels and appearance of vibration which is generated in wheel–rail contacts if the wheel is mounted with a misalignment in the horizontal plane.

Plate box structure made in the form of a flat frame [1] and composed of a beam with a closed profile of cross-section has a very high rigidity of plane displacement, which is deteriorated additionally by the rigidity of joining elements proper made by welding.

This structure promotes the free spreading of a running wave of high-frequency oscillations (vibrations) from the place of their formation (wheel–rail contacts) to different areas of bridge (slipping blocks and site welds of end beams, places of bending the chord plates of end beams and fastening the main beams to end beams), in which the kinetic energy of a running wave is absorbed in stress concentrators of these sub-assemblies, contributing to a gradual accumulation of fatigue damages and formation of cracks.

Similarly, these oscillations are transferred into an upper part of crane beams, causing the rapid damages of welded joints, fastening the chord plate and vertical stiffeners to the wall.

CONCLUSIONS

1. It was established that up to 60 % of travelling cranes have fatigue damages of the span, which are formed, as a rule, in places, where, according to calculations made using generally-accepted procedures, the low level of stresses from loads caused by lifting-lowering the weights and their transportation by carriage along the main beams is formed that is explained by the action of a two-frequency load.

2. The need was stated for a radical revision of approaches to the procedure and principles of designing, manufacture and design of welded structures of crane bridges as regards to assurance of their fatigue resistance.

3. It was found that the fatigue cracks are formed under the action of loads occurring in movement of travelling cranes in the span as a result of appearance of secondary stresses which are not taken in consideration in generally-accepted procedures of strength design.

4. It is most rational to increase the fatigue life of welded crane bridges by improving the travelling properties, i.e. stabilization of the load level, both in vertical and also in horizontal planes that will promote the increase in cyclic fatigue life of the bridge structure.

1. Emelianov, O.A. (2002) *Welded crane bridges. Design, stress loading, diagnostics, service life assurance*. Kramatorsk: DSEA.
2. Zadiraka, V.F., Emelianov, O.A. (1983) About increase in carrying capacity and service life of welded structures of bridge cranes. *Avtomatich. Svarka*, **10**, 52–58.
3. Trufyakov, V.I. (1998) Increase in fatigue resistance of welded joints and structures. *Ibid.*, **11**, 11–19.
4. *RD 50-694–90*. Procedure guidelines. Reliability in technique. Probabilistic method of calculation of welded structure fatigue.
5. Emelianov, O.A., Shepotko, V.P., Lubenets, S.V. et al. (2001) Formation and kinetics of transverse two-frequency loads acting on the welded bridge of crane. *Tekhn. Diagnostika i Nerazr. Kontrol*, **1**, 13–18.
6. Trufyakov, V.I., Dvoretsky, V.I., Mikheev, P.P. et al. (1990) *Strength of welded joints at alternating loads*. Kiev: Naukova Dumka.
7. Kovalchuk, V.S. (1998) Determination of cyclic service life of metals at two-frequency low-cycle loading. *Avtomatich. Svarka*, **9**, 12–14.
8. Fisher, J., Mertz, D. (1985) Cracking in steel bridges. *Grazhd. Stroitelstvo*, **2**, 9–13.
9. Emelianov, O.A. (1997) Crane bridges. In: *Welded structures*. Refer. Book. Kiev: Naukova Dumka.
10. Emelianov, O.A., Zhemchuzhnikov, G.V., Kotenko, E.V. (1976) *Repair of metal structures by electric welding*. Donetsk: Donbass.

DEVICE FOR SINGLE-BUTTON ADJUSTMENT OF OPERATING MODES OF A SEMI-AUTOMATIC WELDING MACHINE

V.A. LEBEDEV, I.S. KUZMIN, V.G. NOVGORODSKY and V.A. TKACHENKO
E.O. Paton Electric Welding Institute, NASU, Kiev, Ukraine

The paper presents one of the methods of construction of operating modes controllers for mechanized arc welding equipment with arc voltage feedback. It is shown that semi-automatic welding machines, operated for a long time, can be upgraded at minimum engineering and hardware costs. This allows improving the welder's labour conditions and welded joint quality.

Keywords: *mechanized welding, modes, control, adjustment, stability, electric drive, current, voltage*

Mechanized arc welding equipment can be upgraded by several methods. Primarily, through introduction of welding technology using, for instance, non-stationary processes [1], as well as development of equipment, which allows facilitating for the welder the problem of selection of optimum welding modes [2]. There also exists a generalized approach to improvement of mechanized arc welding equipment, namely organizing synergic control of the welding process, implemented by semi-automatic machines [3].

As shown by experience, all this is applicable mainly to new models of equipment, namely semi-automatic machines with modern designs of welding current sources, systems of control and adjustment.

On the other hand, the enterprises of Ukraine and CIS countries have a considerable fleet of welding equipment with welding current sources, which may be in service for a long time yet (semi-automatic machines of A547Um type, A825 with VS300 (VS300B) sources, etc.). They can be upgraded to a certain extent at repair, replacement of inoperable components and elements (both mechanical elements of the feed system [4] and adjustment systems).

The purpose of this work is development of engineering solutions for adjustment systems of semi-automatic welding machines, which may significantly increase the effectiveness of their operation, simplify mode selection, and maintain optimum mode relationship, thus facilitating the work of the welder and improving weld quality.

One of the methods simplifying establishment of the modes of operation of welding equipment in the optimum range, is that of single-button control (coordination), which may be implemented by several main methods:

- coordination of welding current and voltage as a result of impact on the welding current source [5];
- coordination of welding current and voltage by acting on the electric drive of the mechanism of electrode wire feed [6].

The first method requires a power source with smooth adjustment of open-circuit voltage. With the second method the welding current source can be of any design, but the mechanism of electrode wire feed should be fitted with a DC power source. Therefore, the second solution is preferable in view of such a diversity and number of semi-automatic machines, already available at the user's disposal, as is may be implemented with the welding current source of any design.

Using any method, it is necessary to assign the level of welding voltage U_w, required for the welding process, and the adjustment system should establish the welding current I_w (optimum) required for this voltage. Such an operation is usually performed through voltage feedback, acting on the adjustable electric drive of the feed mechanism and implementing $I_w = f(U_w)$ dependence. In the simplest case, required for a sound welding process, the above dependence is of a linear nature. It is further taken into account that the welding current and electrode wire feed rate v_f are connected by a linear dependence. The two above conditions may serve as the assumptions taken during consideration of regulator operation by the principle of $I_w = f(U_w)$. Let us emphasize that the considered regulation is implemented due to positive welding voltage feedback.

In work [7] we performed analysis of the regulation system, which implements $I_w = f(U_w)$ dependence. Conditions were determined of stable operation of such a system with minimizing of adjustment errors both by the signal of mode setting, and by the signal of disturbance (variation of voltage of welding current source).

Conducted analysis allows engineering an adjustment system of any complexity and using any element base, which was done at the E.O. Paton Electric Welding Institute. It was taken into account that for solid wire CO_2 welding with other conditions being equal, $I_w = f(U_w)$ dependence can be described by the following linear equation in a certain range of modes:

$$I_w = \frac{U_w - U_{w0}}{k_x},$$

where k_x is the coefficient of the slope of $I_w = f(U_w)$ characteristics; U_{w0} = const.

From the studied range of welding modes it was found that U_{w0} = 15 V, and this is the basis for a substantial simplification of the regulator design. The considered dependence is shown in Figure 1. It should be noted that the slope of $I_w = f(U_w)$ dependence is determined by a number of factors, including electrode wire diameter, kind of shielding gas used for the material being welded, weld position in space, etc.

The problem of engineering implementation of the regulator in the form which is simplest, repeatable and repairable under any conditions, can be solved on the basis of the most readily available component base. This is exactly the original design which is shown in Figure 2.

The regulator is based on an adjustable electric drive on *VD1* thyristor [8] (encircled by a dashed line), powered by a full-wave rectifier with unfiltered output voltage. Negative feedback by voltage on armature of electric motor *M1* is applied to the electric drive. This feedback voltage is compared with the set voltage, established by *R2* resistor. The difference of the above voltages is applied to the control emitter–base junction of *VT1* transistor, is amplified by it and controls thyristor *VD1* so as to maintain the frequency of rotation of the motor shaft (i.e. emf) close to that which is induced by the set voltage. It is obvious that welding current in the starting working point is set (adjusted) by the above resistor. Cutoff voltage (15 V) is adjusted by *R1* resistor. It should be noted that the stabilization voltage of stabilitron *D3* was set at 15 V level. Slope of $I_w = f(U_w)$ characteristic is set by *R3* resistor. Matching the relatively low-level

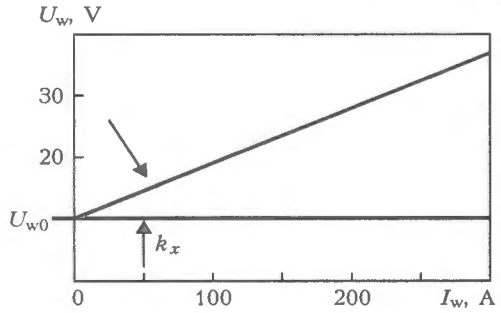

Figure 1. Dependence $I_w = f(U_w)$ at U_{w0} = 15 V

set voltage to the armature voltage of the electric motor is performed by a divider, which consists of resistors *R8* and *R9*. This divider is connected to thyristor *VD1* by bridge *A*. When the thyristor is unblanked, bridge *A* does not fulfill any functions, and during its blanked condition motor emf is tapped by bridge *A* through divider *R8* and *R9* into the feedback circuit for comparison with the set voltage.

Diode *D1* enables the current of the unblanked thyristor to flow directly to the motor armature, bypassing divider *R8* and *R9*, i.e. is not weakened by the latter.

Capacitor *C1* together with resistor *R4* to a certain extent eliminates the drawbacks inherent in the selected simple thyristor circuit of the electric drive (i.e. at low frequencies of rotation of the motor shaft its jogging is eliminated, which could result from the mode of thyristor drive operation in the zone of intermittent currents).

A structure consisting of resistors *R5, R6, R7* and capacitor *C3* corresponds to that of passive integrating circuit, namely a filter considered above. In addition, this filter further serves as a means of filtering voltage spikes, resulting from operation of a source of welding current and physical phenomena during the arc process.

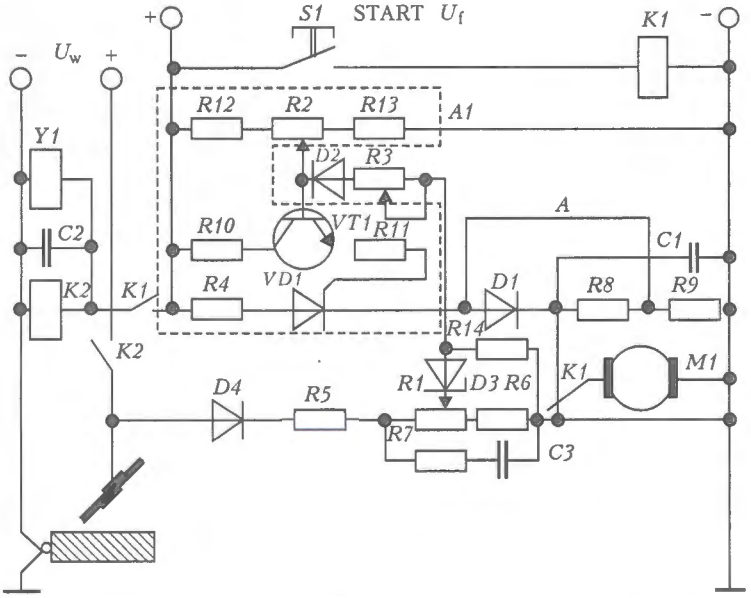

Figure 2. Elementary diagram of the system of arc process regulation by the principle of single-button control using an adjustable thyristor electric drive: *K1, K2* — control relay; *Y1* — gas valve (other designations except for those given in the text are matching and decoupling elements)

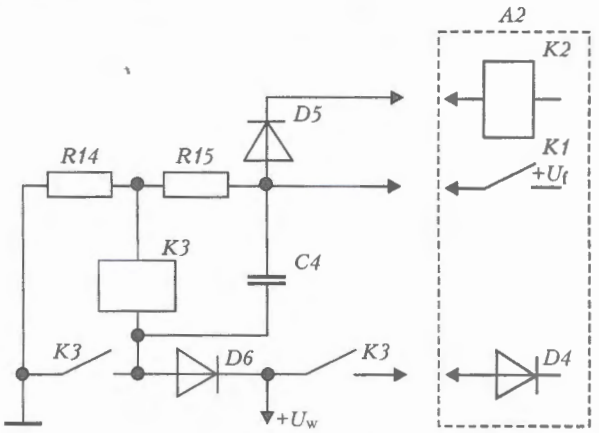

Figure 3. Elementary diagram of a device, which eliminates electric drive operation at higher rates of electrode wire feed (other designations except for those given in the text are matching and decoupling elements)

The proposed regulator in its full circuit volume was tested with several models of semi-automatic welding machines, which have operated for a long time already under different conditions and performed various operations. These are semi-automatic machines A547Um, A825, A1230 with D90, SL570S, KPA561 motors, respectively. Welding current sources of VS300, VS300B, VDG303 type were used. In all the cases the anticipated results were obtained, which were highly estimated by welders, who used only setting of open-circuit voltage of welding current sources, when changing the mode. The range of adjustment of the rotation frequency of driving motor shaft, generated by the thyristor electric drive included into the mode regulator, is quite sufficient for supporting the welding modes, given in the certificates of the semi-automatic machines, and in a number of cases it is even 1.2–1.5 times higher than these parameters.

Such an adjustment system in a somewhat truncated form was tested, when incorporated into the semi-automatic machines, having their own electric drives. Semi-automatic machines of PDG312, PDG516 types are fitted with welding current sources with a smooth adjustment of output voltage. This provides a solution of the problem of interfacing the adjustable electric drives of the semi-automatic machines (electric drives of BUSP-2 systems) with the device for isolation of a signal of positive feedback by welding voltage. Such upgrading of the semi-automatic machine is effective.

It can be further noted that in some cases the circuit of the semi-automatic machine has a feature, which not all of the welders regard as positive (Figure 2). It consists in that if the welding process does not reach the steady state for a long time (electrode wire edge is far from the point of electrode touching the metal, etc.), positive feedback voltage, proportional to the open-circuit voltage of the welding current source, allows the electric drive to feed electrode wire at a somewhat higher rate. The above problem is present in any engineering solution related to such an organization of feedbacks. It can be solved by various methods, including application of welding current sensors.

For this case, allowing for the principle of minimum engineering and hardware costs, a device in Figure 3 was proposed, which provides a quite simple solution for eliminating the above drawback. Figure 3 also shows a variant of connection of the device to the regulator (see Figure 2). Let us consider the operation of this device. Here *A2* denotes the regulator elements (see Figure 2). Welding voltage feedback circuit is connected to electric drive input through contact of relay *K3* (connection to circuit of diode *D4*) at operation of relay *K3*. When working cycle of the semi-automatic machine is switched on, voltage $+U_f$ is applied through contact of relay *K1* to the circuit of coil of relay *K1*. The latter does not operate as the fed voltage $+U_f$ is compensated by voltage $+U_w$ present on the cathode of decoupling diode *D6*. When electrode wire touches the workpiece, the voltage of welding current source drops markedly, i.e. $U_w \rightarrow 0$, and potential difference in the winding of relay *K3* is sufficient for its operation. While operating, relay *K3* with its contacts goes into the self-holding mode and remains switched on during the entire welding cycle, thus providing the operation of welding voltage feedback circuit. Capacitor *C4* is used for guaranteed

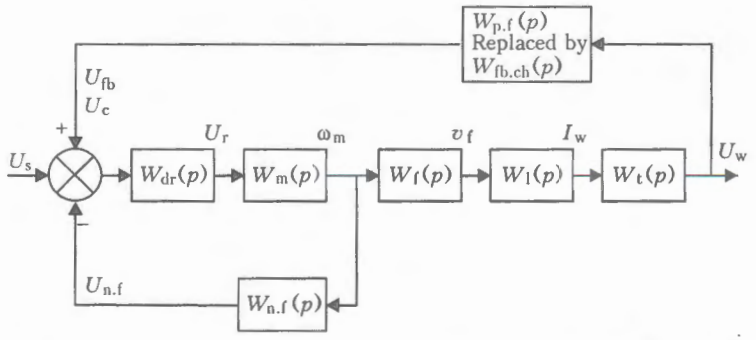

Figure 4. Block diagram of an arc process regulator in consumable electrode mechanized arc welding: $W_m(p)$ is the transfer function of DC motor; $W_{dr}(p)$ is the transfer function of the regulator of rotation frequency of motor shaft (electric drive); $W_{p.f}(p)$ is the transfer function of positive feedback by welding voltage; $W_f(p)$ is the transfer function of electrode wire feed mechanism; $W_l(p)$ is the transfer function of a link, determining $I_w = f(v_f)$ dependence; $W_{n.f}(p)$ is the transfer function of a negative feedback circuit, which stabilizes the rotation frequency of driving electric motor shaft; $W_t(p)$ is the transfer function of a link, determining $I_w = f(U_w)$ dependence; U_s is the set voltage; U_{fb} is the feedback voltage; U_c is the control voltage; U_r is the regulator voltage; ω_m is the frequency of motor shaft rotation; v_f is the electrode wire feed rate; $W_{fb.ch}$ is the changed feedback transfer function

switching on of relay *K3* at a short period of the initial short-circuiting of welding circuit. Effectiveness and reliability of operation of the above circuit has been verified both when operating as part of a regulator of working modes of a semi-automatic welding machine, and various devices, controlling the moment of welding arc excitation.

Selection of the regulator circuit parameters can be performed by studying the transfer function of the system of adjustment for stability, accuracy with the required correction links, etc., which is derived in keeping with the block diagram shown in Figure 4.

It should be noted that it was exactly studying the regulator structure, which defined the need for incorporating a passive integrating filter with the required parameters into the regulator circuit.

One of the main problems defined for development of the regulator circuit, was that of provision of the maximum possible simplicity and accessibility at repetition. The same engineering solutions can form the basis for developments using other sets of components for application in batch-produced welding equipment.

For new developments we recommend using one of the versions of ZELIO programmable controller as both the regulator and sequential control unit, which is relatively easily programmable and serviceable by the staff of practically any modern enterprise.

1. Paton, B.E., Voropaj, N.M., Buchinsky, V.N. et al. (1977) Arc welding process control by programming of electrode wire feed rate. *Avtomatich. Svarka*, **1**, 1–5, 15.
2. Podola, N.V., Rudenko, P.N., Kobylin, A.M. (1993) Semi-automatic machine for mechanized welding with single-button control. *Ibid.*, **11**, 42–44.
3. Lucas Head, W., (1985) Synergic pulsed MIG welding process, equipment and application. *FWP J.*, 25(**6**), 7–23.
4. Lebedev, V.A., Pichak, V.G. (2000) A new approach to design of the electrode wire feed mechanism. *The Paton Welding J.*, **4**, 33–36.
5. Lebedev, V.A. (1990) Coordinated control of semi-automatic welding machine operating modes. *Avtomatich. Svarka*, **12**, 56–59
6. Pokhodnya, I.K., Shlepakov, V.N., Suprun, S.A. et al. (1975) Automatic control of flux-cored wire welding conditions. *Ibid.*, **7**, 35–36.
7. Lebedev, V.A., Kuzmin, I.S., Novgorodsky, V.G. (2002) Control of mechanized consumable-electrode arc welding process with optimum ratio of welding parameters. *Tekhnologiya Metallov*, **1**, 12–17.
8. Lebedev, V.A., Poloskov, S.I., Bratchuk, S.D. (2002) Functional peculiarities of DC electric drives for welding equipment. *Svarochn. Proizvodstvo*, **6**, 34–41.

THESIS FOR SCIENTIFIC DEGREE

Ryabtsev A.D. «Electroslag Remelting of Metals and Alloys in Chamber-type Furnaces using Fluxes with Active Additions». Thesis for scientific degree of Dr. of Technical Sciences on specialty «Metallurgy of high-purity metals and special alloys». The E.O. Paton Electric Welding Institute of the NAS of Ukraine, Kiev, 2004. Date of defence is 17 March, 2004. The work was carried out at Donetsk National Technical University.

Thesis is devoted to the development of theoretical fundamentals of chamber electroslag remelting (CESR), study of its main laws, creation and realization of technologies of producing high-quality ingots from different metals and alloys.

In the work, the physical-chemical, electrical and heat peculiarities of CESR using fluxes of CaF_2–Ca system were investigated.

It was established that additions of metal calcium to the flux leads to the ESR transition to the instable arc region at a level of a coefficient of harmonics within 25–30 %. Data were obtained about the electroconductivity of fluxes of CaF_2–Ca system under the CESR conditions (19–23 $Ohm^{-1} \cdot cm^{-1}$ at temperatures of the process from 1920 to 2170 K and 3–15 wt.% Ca content).

For the CESR conditions the optimum contents of metal calcium, from the point of view of adaptability and depth of metal refining, were determined using slags of CaF_2–Ca system, which depend on process temperature and are in the range from 2 to 6 wt.%. The feasibility of refining, modifying and microalloying with metal calcium of steels of different classes in CESR using flux of CaF_2–Ca system is shown.

Mechanisms of removing inclusions of titanium nitride from titanium and titanium alloys in CESR are theoretically grounded and confirmed experimentally. Technology of refining titanium and its alloys from nitride inclusions has been developed, providing the damage of inclusions at 0.7–1.1 mm/s rate.

Using the given technology, the batch of ingots from titanium alloy VT6-4 was melted for company «General Electric» (USA). Results of metal tests confirmed the high efficiency of the technology that allowed company «General Electric» to recommend it for industrial testing at some enterprises of the USA and West Europe.

The feasibility of alloying steel and titanium with nitrogen is shown in electroslag remelting in a chamber furnace in argon atmosphere at 101 kPa pressure using the Ca-containing flux.

Challenging directions in use of the developed technology for the production of ingots of titanium γ-aluminide and alloys of Fe–Nd–B system are considered.

Design solutions without high investments are offered for re-equipping of existing ESR installations into chamber-type electroslag furnace, providing the controllable furnace atmosphere. The industrial shop bay of chamber-type ESR furnaces has been firstly created at NPO «Tulachermet» in the former USSR.

The new technological process of producing metals and alloys on the base of a chamber electroslag remelting and use of reactive metal-containing fluxes became the basis on an innovation project involved into «Program od scientific-technical progress of Donetsk region for the period till 2020», approved by the Decree of the President of Ukraine of 25.05.2001.